NAVAL POSTGRADUATE SCHOOL

MONTEREY, CALIFORNIA

THESIS

INCREASING ENDURANCE IN TACTICAL DC MICROGRIDS WITH VARIABLE GAIN DROOP CONTROL

by

John E. Dommert

September 2019

Thesis Advisor: Giovanna Oriti
Co-Advisor: Roberto Cristi

THIS PAGE INTENTIONALLY LEFT BLANK

REPORT DOCUMENTATION PAGE			*Form Approved OMB No. 0704-0188*

1. AGENCY USE ONLY *(Leave blank)*	**2. REPORT DATE** September 2019	**3. REPORT TYPE AND DATES COVERED** Master's thesis

4. TITLE AND SUBTITLE
INCREASING ENDURANCE IN TACTICAL DC MICROGRIDS WITH VARIABLE GAIN DROOP CONTROL

5. FUNDING NUMBERS

6. AUTHOR(S) John E. Dommert

7. PERFORMING ORGANIZATION NAME(S) AND ADDRESS(ES)
Naval Postgraduate School
Monterey, CA 93943-5000

8. PERFORMING ORGANIZATION REPORT NUMBER

9. SPONSORING / MONITORING AGENCY NAME(S) AND ADDRESS(ES)
N/A

10. SPONSORING / MONITORING AGENCY REPORT NUMBER

11. SUPPLEMENTARY NOTES The views expressed in this thesis are those of the author and do not reflect the official policy or position of the Department of Defense or the U.S. Government.

12a. DISTRIBUTION / AVAILABILITY STATEMENT
Approved for public release. Distribution is unlimited.

12b. DISTRIBUTION CODE
A

13. ABSTRACT (maximum 200 words)

Current tactical microgrids range from dozens of diesel generators to small solar panels. Projected operational concepts greatly reduce the size and change the mission of these bases from the previous paradigm. With more mobile basing, the integration of novel control architectures based on efficiency presents an opportunity for greater operational endurance from reduced fuel consumption and smaller physical footprints. To form these microgrids, diesel generators have been used for decades and are proven to be a reliable and flexible power source. Tactical power systems employed today are only in the early stages of leveraging the benefits of parallel generation used in industry. Droop control is currently one of the industry standards for operating parallel generators. By optimizing the underlying architecture of droop control methods, paralleled generators can achieve greater efficiency and mission flexibility. This thesis will model a small-scale mobile microgrid using an optimized droop control scheme to achieve an optimal power dispatch with respect to efficiency. Optimal dispatch was determined using the combined generator fuel consumption as a function of the output power. The optimal dispatch was achieved by deriving the corresponding droop gains.

14. SUBJECT TERMS
generators, efficiency, droop control, optimization, tactical power

15. NUMBER OF PAGES
97

16. PRICE CODE

17. SECURITY CLASSIFICATION OF REPORT	**18. SECURITY CLASSIFICATION OF THIS PAGE**	**19. SECURITY CLASSIFICATION OF ABSTRACT**	**20. LIMITATION OF ABSTRACT**
Unclassified	Unclassified	Unclassified	UU

NSN 7540-01-280-5500

Standard Form 298 (Rev. 2-89)
Prescribed by ANSI Std. 239-18

THIS PAGE INTENTIONALLY LEFT BLANK

Approved for public release. Distribution is unlimited.

INCREASING ENDURANCE IN TACTICAL DC MICROGRIDS WITH VARIABLE GAIN DROOP CONTROL

John E. Dommert
Captain, United States Marine Corps
BS, Virginia Military Institute, 2013

Submitted in partial fulfillment of the
requirements for the degree of

MASTER OF SCIENCE IN ELECTRICAL ENGINEERING

from the

NAVAL POSTGRADUATE SCHOOL
September 2019

Approved by: Giovanna Oriti
Advisor

Roberto Cristi
Co-Advisor

Douglas J. Fouts
Chair, Department of Electrical and Computer Engineering

THIS PAGE INTENTIONALLY LEFT BLANK

ABSTRACT

Current tactical microgrids range from dozens of diesel generators to small solar panels. Projected operational concepts greatly reduce the size and change the mission of these bases from the previous paradigm. With more mobile basing, the integration of novel control architectures based on efficiency presents an opportunity for greater operational endurance from reduced fuel consumption and smaller physical footprints. To form these microgrids, diesel generators have been used for decades and are proven to be a reliable and flexible power source. Tactical power systems employed today are only in the early stages of leveraging the benefits of parallel generation used in industry. Droop control is currently one of the industry standards for operating parallel generators. By optimizing the underlying architecture of droop control methods, paralleled generators can achieve greater efficiency and mission flexibility. This thesis will model a small-scale mobile microgrid using an optimized droop control scheme to achieve an optimal power dispatch with respect to efficiency. Optimal dispatch was determined using the combined generator fuel consumption as a function of the output power. The optimal dispatch was achieved by deriving the corresponding droop gains.

THIS PAGE INTENTIONALLY LEFT BLANK

TABLE OF CONTENTS

LIST OF FIGURES

THIS PAGE INTENTIONALLY LEFT BLANK

LIST OF TABLES

THIS PAGE INTENTIONALLY LEFT BLANK

LIST OF ACRONYMS AND ABBREVIATIONS

A	amperes
AC	alternating current
COP	combat outpost
DC	direct current
DoD	Department of Defense
EABO	Expeditionary Advanced Basing Operations
EMS	Energy Management System
Hz	hertz
kW	kilowatt
PWM	Pulse Width Modulation
RMS	root-mean squared
USMC	United States Marine Corps
V	volts

THIS PAGE INTENTIONALLY LEFT BLANK

ACKNOWLEDGMENTS

Thank you to my advisors, Dr. Giovanna Oriti and Dr. Roberto Cristi, for their direction and support. Their willingness to invest time and provide guidance was evident and genuine during the entire process. Thank you for providing the resources to complete this thesis and grow as a student.

The foundation for where I am today is a product of my diligent and loving parents. Your teaching and training have guided me through life and this experience. Thank you to my brother for being a role model and pioneer. I am a benefactor of your life lessons and example.

Last, I would like to thank my wife, who sustains unwavering support and devotion. You're an incredible woman and teammate. Everything we do, we do and achieve together.

THIS PAGE INTENTIONALLY LEFT BLANK

I. INTRODUCTION

A. MOTIVATION

The United States has entered the era of "strategic competition" with peer competitor state actors vying for the position of global leader [1]. In this strategic environment, the risks associated with perceived acts of war and the subsequent conflict are great. This presents a need for smaller forces with strategic relevance both to prevent conflict and dominate the battlespace if one should occur. Additionally, large-scale conflicts create a significant drain on national resources, especially in the energy sector [2]. For the United States Marine Corps (USMC), one answer to these challenges has materialized through Expeditionary Advanced Base Operations (EABO), which "seeks to further distribute lethality by providing land-based options for increasing the number of sensors and shooters beyond the upper limit imposed by the quantity of seagoing platforms available. The EABO concept espouses employing mobile, relatively low-cost capabilities in austere, temporary locations forward as integral elements of fleet/JFMCC operations" [3]. The description is explicit on force structure and maneuver aspects, while it is implicit on the need for mobile and energy efficient systems to support them.

One component to achieving these low-cost, mobile capabilities is through continued innovations in the use of operational energy. Title 10 defines operational energy as the "energy required for training, moving, and sustaining military forces and weapons platforms for military operations. This term includes energy used by tactical power systems and generators, as well as by weapons platforms themselves" [4]. Generators have and continue to be the most reliable method of providing electrical energy to ground forces. Previous improvements on these systems have focused on mostly stationary systems for larger forces (>120 personnel). To provide the reduced logistical burden and support increased decentralization of forces, future improvements must be flexible in mission sets and how they achieve higher efficiency.

B. RESEARCH OBJECTIVES

The primary objective of this research is to present a framework for efficient usage of tactical generators in order to minimize overall fuel consumption. Increased fuel efficiency results in longer sustained operations and reduced logistical requirements. Efficiency gains must not decrease generator performance or stability. Considerations for maintenance and emissions were not considered.

While the primary objective is efficiency, any design solution must consider the requirements of the end-user, the operational environment, and the acquisition process. First, any changes needed to have little to no impact on how the uniformed operator employed the generator. Service members have a rigid training structure and curricula; additional complexity in end-user operations create a barrier for adoption and effective employment. Second, the operational environment requires mobility and flexibility in power supplies. The configuration of power generation needs to be transportable via lightweight tactical vehicles and provide power over a wide band of outputs. Last, new and unproved technologies take significantly longer to complete the acquisition process than legacy systems. Any method to gain efficiency needs to leverage existing systems currently fielded. This thesis addresses these issues through the implementation of a modified droop control and generators of different power ratings.

C. RELATED WORK

Previous theses have been written on reducing tactical generator fuel consumption based on a variety of methods to include load matching, load shedding, and generator scheduling. Kelly [5] discussed the use of an Energy Management System (EMS) to select to the most efficient generator for use at a given power requirement. The control decision for a given generator was binary, on or off. In [6], Garcia utilized mixed integer linear programming to show that using generators of varying sizes presents efficiency gains based on different efficiencies for a given load. Several papers have been written on how to actually implement the above concepts using optimal dispatch. Optimal dispatch is proposed in [5]–[9] based on load matching and shedding. A cost-based approach was used in [10]–[12] for optimal dispatch via droop control. The primary difference between the

two methods lies in the continuous nature of the control. Load matching optimization ([5]–[9]) focuses on a binary decision for each generator where droop control optimization ([10]–[12]) proposes an optimal solution that is continuous for each generator.

THIS PAGE INTENTIONALLY LEFT BLANK

II. BACKGROUND

A. CIRCUIT BASICS

The governing equations for the circuit analysis are derived from Ohm's Law, Kirchhoff's Current Law (KCL), and conservation of power. Ohm's law,

$$V = IR, \tag{1}$$

states that voltage is the product of a resistance and the current through that resistance. KCL, given by

$$\sum_{j=1}^{n} i_j = 0, \tag{2}$$

states that the sum of all currents at a node must equal zero or that sum of the currents entering a node must equal the sum of the currents leaving a node. Conservation of power states the sum of the power entering a system must equal the sum of the power leaving a system, whether through work or losses. Power is defined as

$$P = VI, \tag{3}$$

and the summation of power is given by

$$P_{total} = \sum_{j=1}^{n} P_j . \tag{4}$$

Integrating (3) gives the energy produced or consumed,

$$E = \int_0^{\tau} P dt . \tag{5}$$

B. GENERATOR BASICS

Generators are variable in size and use different technologies, but fundamentally all convert mechanical energy into electrical energy. The DoD primarily uses diesel generators to produce electrical energy in remote locations. Diesel generators function like an automotive engine, using combustion of liquid fuel to create rotational motion. Diesel-

electric generators have a rotor, attached to the rotational shaft, and stator, attached to the generator body. These two components allow the generator to create current from a spinning shaft. The rotor shown in Figure 1 contains coils that are excited by a DC source. The current flowing through the coils generates a magnetic field that intersects the coils on the stator. When the rotor rotates, the magnetic field from its coils induces an alternating voltage in the stator coils. Once the generator output terminals are connected to an electrical load, a corresponding current will flow to the load. As the electrical load increases, the generator controller increases the fuel rate into the combustion chamber to keep up with demand. The increase in fuel consumption does not increase linearly with the load. Figure 2 shows a characteristic curve for diesel generator efficiency [13]. The plot shows efficiency, in percentage, as a function of the generator load capacity or how much total power it can provide. More specifically, efficiency will be defined in energy delivered for every gallon of fuel consumed (kWh/gal).

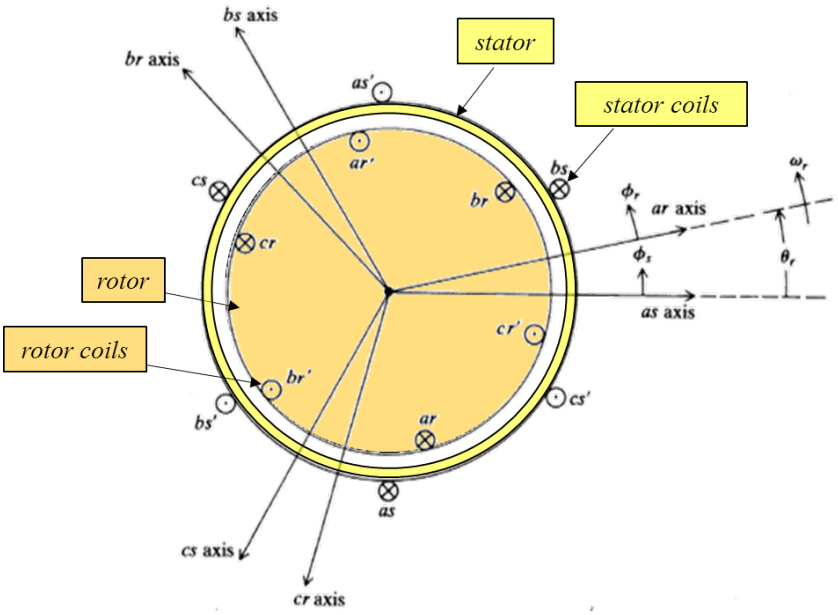

Figure 1. Generator Rotor and Stator Diagram. Adapted from [14].

Figure 2. Characteristic Curve for Generator Efficiency. Adapted from [13].

C. MICROGRID CONTROL LEVELS

A microgrid is an electrical power system, smaller than the utility grid, but still consisting of power generation and loads. This system has multiple layers of control governing behavior at each layer. One common architecture classifies the whole system into three layers: primary, secondary, and tertiary. Primary controllers are the lowest level controlling the function on an individual source which entails voltage and frequency regulation. If only one generator is present, no other control levels are needed. With multiple generators, a secondary controller is added. The secondary controller regulates the output of the system and provides a new input to the primary controllers, allowing the two distinct system to work in unison. The secondary controller has a larger time constant and reacts more slowly than the primary controller. If the secondary controller responds too quickly, the primary controller may never reach a quasi-steady state and the system may become unstable. Both primary and secondary controllers usually operate on set parameters and may be tuned during operation. A tertiary controller may be added to accomplish higher level decisions and regulation. In some cases, the tertiary controller allows the

microgrid to connect or disconnect from the larger utility grid. In this thesis, the tertiary controller optimizes the power distribution among the generators.

D. DROOP CONTROL

Droop control operates on the basic principle that multiple generators operating in parallel will share load requirements based on their individual rating [15]. In a DC system, the term droop refers to the allowable deviation in output voltage for a given generator. Figure 3 shows a simplified block diagram of two generators operating in parallel. Figure 4 shows how droop control for the two DC generators is implemented.

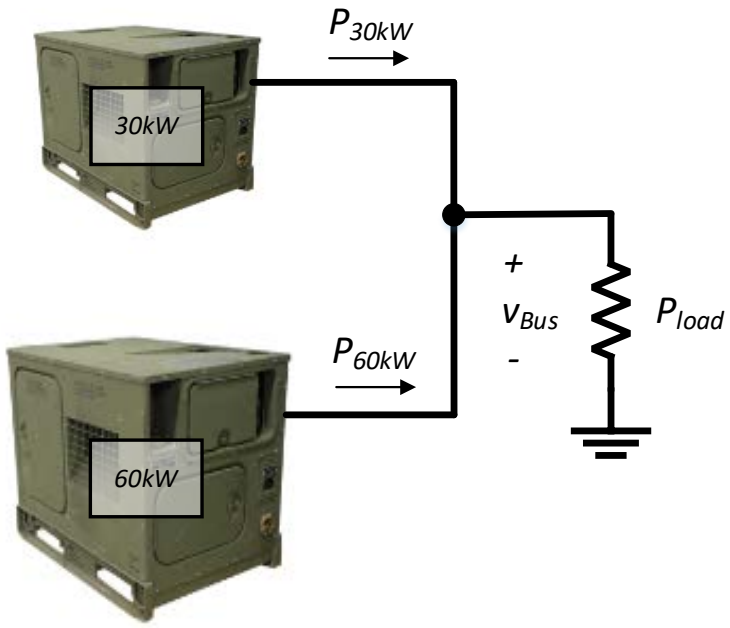

Figure 3. Parallel Generators

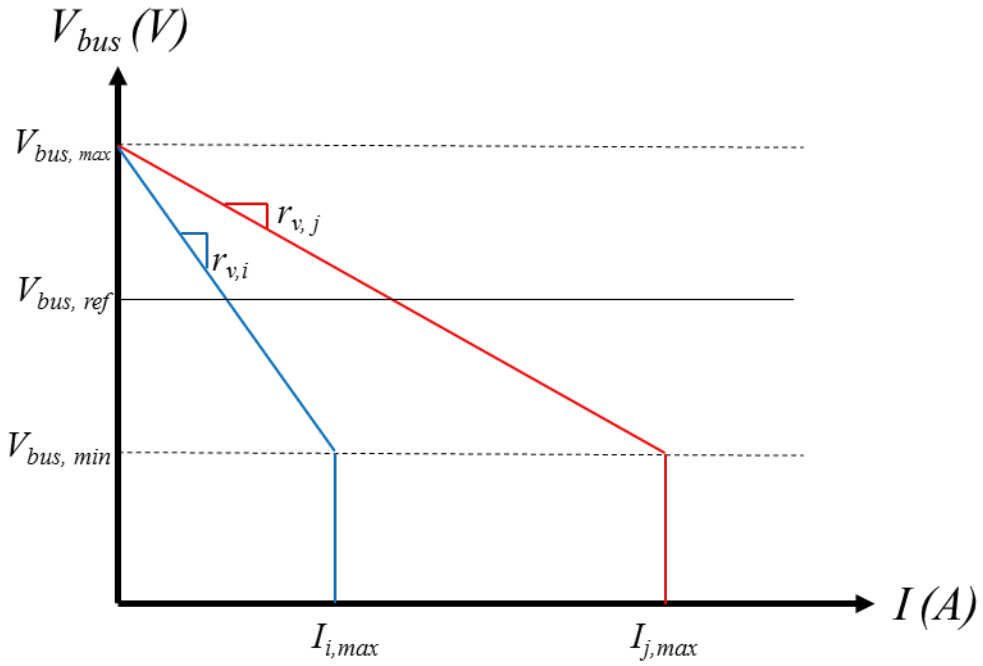

Figure 4. Droop Control Virtual Resistances

The two lines shown in Figure 4 represent one generator each and the range along which the voltage and current fluctuate. The output voltage will "droop" up and down along these lines. The blue line represents the smaller of the two generators. Between the two generators, a common maximum and minimum bus voltage are utilized. An electrical bus is a physical cable or bar which provides a common point for components to connect. The maximum current is based on the power rating of the combined generators. Figure 4 shows a constant slope, r_v ,across the whole range of output currents. The slope is calculated as

$$r_{Vi} = \frac{V_{bus,\max} - V_{bus,\min}}{i_{i,\max}}. \tag{6}$$

The commanded voltage to the generator voltage control is found using the equation of the line from Figure 4,

$$V_{bus,ref} = V_{bus,\max} - r_{v,i} I_{i,\max}. \tag{7}$$

Using Figure 3 and (7), a control loop is created which integrates (6) as a feedback gain. Figure 5 shows the primary controller for each generator.

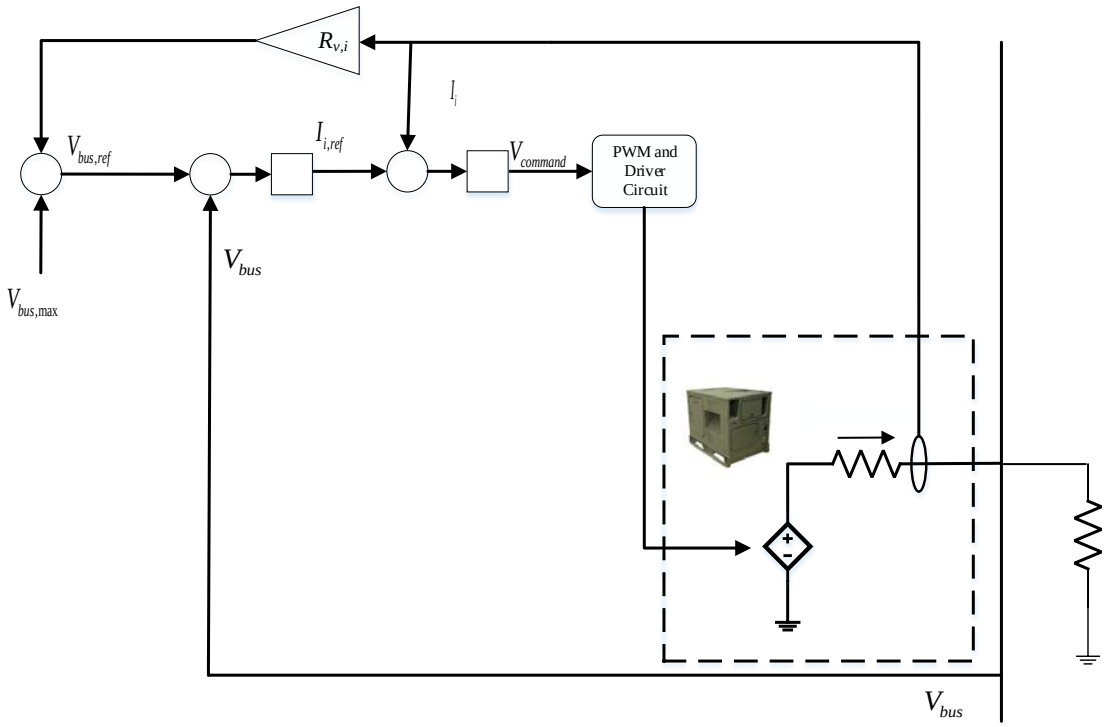

Figure 5. Primary Droop Control. Adapted from [15].

The generator is modeled as a dependent voltage source with a series resistance. This is a generic, DC source model and can be applied to any DC source (generator, turbine, battery, etc.). A current sensor detects the generator output current and sends it to the inner current controller and the outer voltage controller as well. A voltage sensor detects the bus voltage and sends it to the outer voltage controller. The Pulse Width Modulation (PWM) and circuit driver are the physical coupling between the controller and the generator. This will vary based on the commercial manufacturer but it sends the actual signals that control the combustion process and excitation voltage. The combustion process will regulate the rotor speed while the excitation voltage will regulate the output voltage.

A secondary controller is added for multiple generators to regulate the bus voltage and keep it at the desired set point. Figure 6 and (8) show how the secondary controller impacts the control equations. Figure 7 shows the control architecture for two parallel generators with the addition of the secondary controller.

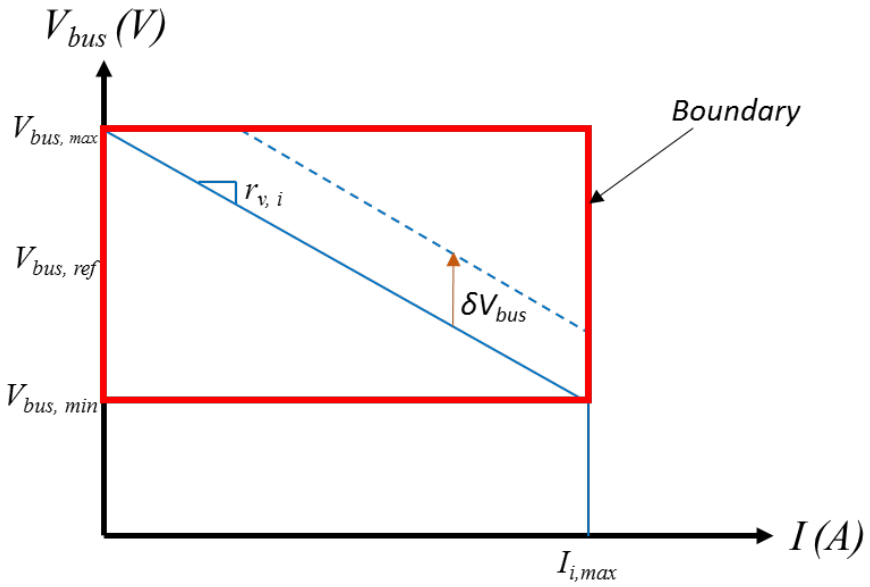

Figure 6. Current-Voltage Line with Secondary Controller

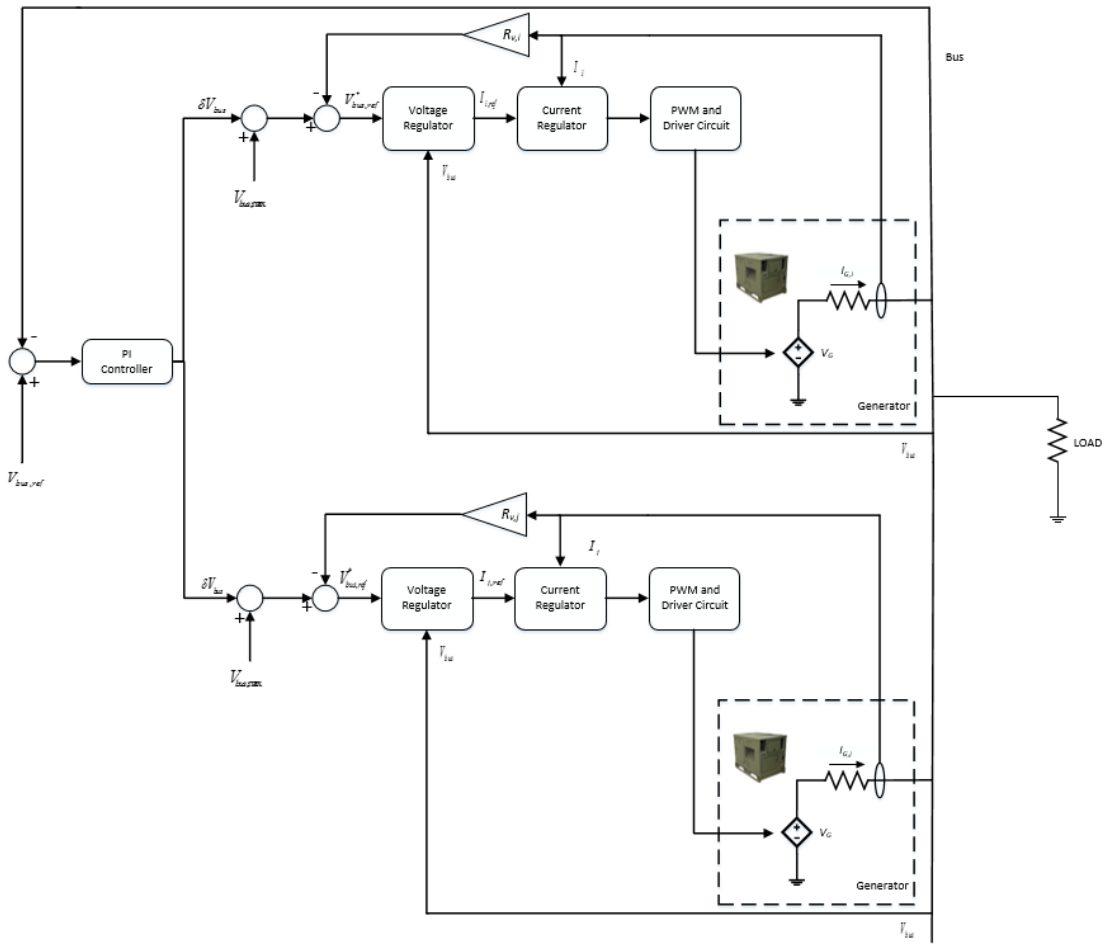

Figure 7. Droop Control with Secondary Controller. Adapted from [15].

δV_{bus} is no-load voltage ($V_{bus,max}$) offset and the new commanded voltage for the generator is

$$V_{bus,ref} = V_{bus,\max} + \delta V_{bus} - r_{v,i} I_{i,\max} . \quad (8)$$

Operating the generators in parallel with no secondary controller creates issues with stability and transients as both dynamics affect the system. The secondary controller gives direct control over the bus voltage and reduces transients by damping the response prior entering the primary controller for the individual generators. With the secondary controller implemented, multiple generators can be paralleled to the same bus with the same control architecture depicted in Figure 7.

III. METHODOLOGY

A Simulink model was created based on Figure 8, a simplified block diagram representing Figure 7, to simulate system response to variable droop gains, generators cycling, and fluctuating loads. The simulation spans a 24-hour time period with a representative load for a small-scale military combat outpost (COP). Two generators are connected in parallel as discussed in Section II.

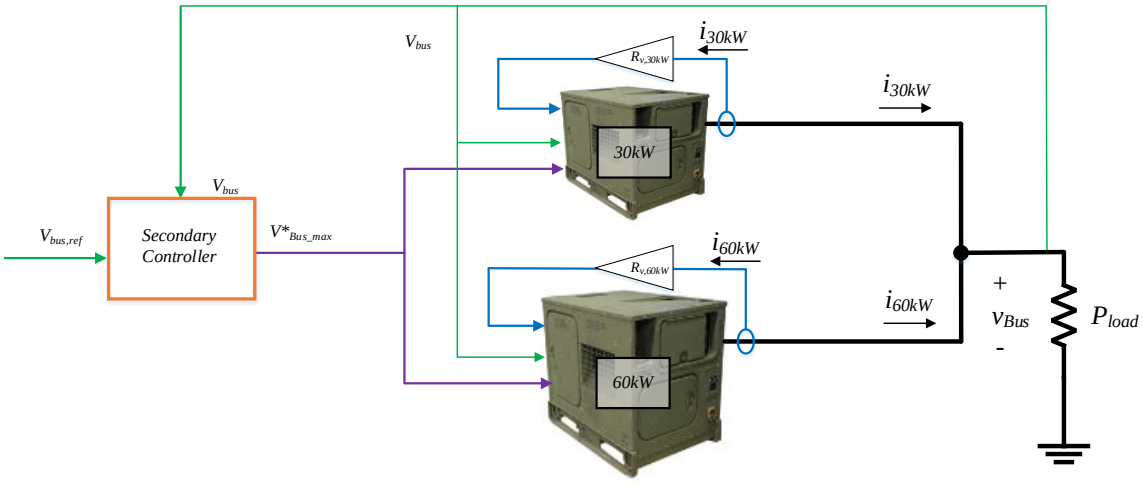

Figure 8. Simplified Block Diagram

A. ASSUMPTIONS

The system modeled is a tactical microgrid for use in mobile applications. The configuration and control law is intended to give flexibility in different mission sets, meaning the generators will operate throughout the set of all possible power outputs. The microgrid analyzed contains two diesel generators, 1–60 kW and 1–30 kW. Fuel consumption rates are assumed to be only a function of load requirement and independent of generator run hours or climate. The maximum load was not allowed to exceed 95% of the system capacity.

The modeled system implements a control architecture for DC generators while current DoD generators are 3-phase AC machines. The purpose of this research was to

introduce the concept of load distribution as a function of efficiency rather than capacity rating. As such, a level of analysis was removed to isolate the optimization component of the problem while still capturing a reduced fidelity approximation of system behavior. This generic model can be used for other DC sources such as batteries or solar panels with a regulated output.

The primary controllers contain inner loop current controllers and outer loop voltage controllers. For simulation, the inner loop current controller was removed as the simulation covered a 24-hr period and the reference current from the voltage controller was assumed to be the output of the current controller. The tertiary controller utilizes inputs from offline optimization and does not use real-time communication between generators. Internal generator losses and line losses were considered to be zero.

B. OPTIMIZATION METHOD

As discussed in Section II, diesel generators have non-linear efficiency curves as well as varying efficiency curves based on their power rating. Figure 9 shows the efficiency curves in kWh/gal for different generators.

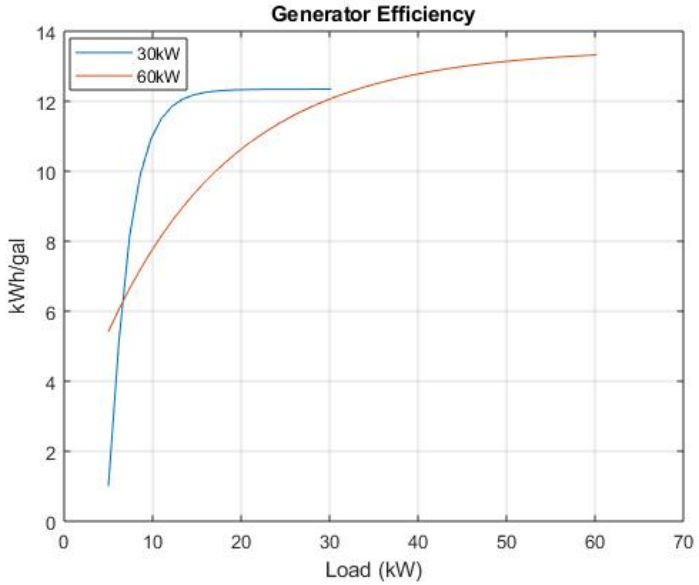

Figure 9. Fuel Efficiency for 30 kW and 60 kW Generators

Each generator has a region where it is more efficient than the other. This creates space to optimize the dispatch of power. In droop control, the virtual resistance, r_V, is proportional to the rated value of the generator and can be used to control the ratio of power output among the generators in the system. By varying this ratio as a function of the load power and efficiency, the optimal dispatch of power, with respect to fuel consumption, can be achieved.

From Figure 8, P_{30kW} and P_{60kW} are the output power, i_{60kW} and i_{30kW} are the output currents, and $R_{V,30kW}$ and $R_{V,60kW}$ are the virtual resistances. P_{load} is the total load requirement and V_{bus} is the DC bus voltage. P_{load} is the sum of P_{30kW} and $P_{60kW,}$

$$P_{load} = P_{30kW} + P_{60kW} . \tag{9}$$

Redefining the generator power with respect to a single variable, γ, yields

$$P_{30kW} = \gamma \cdot P_{load} \ , \ P_{60kW} = (1-\gamma) \cdot P_{load} . \tag{10}$$

Since each generator references the same voltages when deriving r_V as seen in (6), the individual values can be written as a ratio where

$$\frac{R_{v,30kW}}{R_{v,60kW}} = \frac{P_{60kW}}{P_{30kW}} . \tag{11}$$

Combing (10) and (11), the following relation forms:

$$R_{v,60kW} = R_{v,30kW} \cdot \left(\frac{\gamma}{(1-\gamma)} \right). \tag{12}$$

By using a nominal value for $R_{v,30kW}$, γ now becomes the control variable to achieve the optimal dispatch between the generators. To analyze γ, the generator fuel consumption was modeled with a linear function

$$C_i(P_i) = b_i + m_i \cdot P_i \tag{13}$$

where i = 30 kW, 60 kW and $C_i(P_i)$ is fuel consumption in gal/hr. Using (10) the cost for each generator is written as

$$C_{30kW}(\gamma, P_{load}) = b_{30kW} + m_{30kW} \cdot \gamma P_{load}, \tag{14}$$

and

$$C_{60kW}(\gamma, P_{load}) = b_{60kW} + m_{60kW} \cdot (1-\gamma) P_{load}, \tag{15}$$

which combine to create

$$C_{total} = C_{30kW} + C_{60kW}. \tag{16}$$

Minimizing (16) as a function of γ for P_{load} > 60 kW gives the optimal dispatch in this region. The minimal value for γ was found for each integer value of P_{load} by iterating values for γ, where 0 < γ < 1. A continuous value of γ if achieved through interpolation between values and shown in Figure 10.

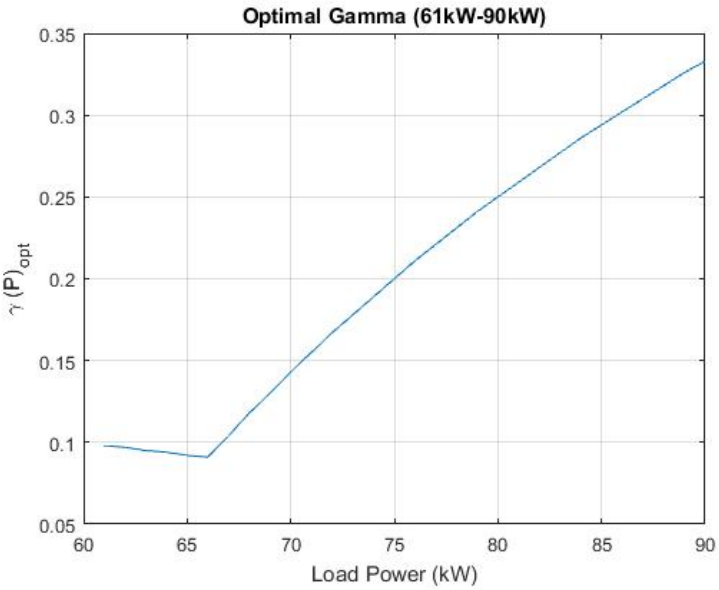

Figure 10. γopt, Pload > 60 kW

The optimization is trivial for P_{load} < 60 kW, as the 30 kW generator is more efficient for the entirety of its load spectrum, while the 60 kW generator is more efficient for values greater than 30 kW, as demonstrated in Figure 9. The optimization leads to one generator on and one generator off for P_{load} < 60 kW. The drawback to this method is the

introduction of transients and generator maintenance concerns with generators cycling on and off [5], [9]. Several methods account for this issue which include scheduling [9] or an energy management system with storage to insure uninterrupted power [5]. This thesis addresses the issue of transients through hand-off or buffer regions. These regions are established based on a 20% spinning reserve for the generator currently operating.

A spinning reserve refers to the available capacity of the generator and the physical inertia of the generator fly wheel. At 80% capacity, the generator still has the ability to provide current in case of surges. Signaling the second generator to turn on at 80% of the current generator capacity gives time for it to spin up and contribute to or take the load. An optimal dispatch for the entire load profile is created using Figure 11 and the before-mentioned logic. Figure 12 shows what each generator will deliver as a function of the load power. There are 5 distinct regions shown in Figure 12 and Table 1 defines the regions and their bounds. Figure 12 combines (16) and Figure 11 to produce the cost of operation in gal/hr for the optimal configuration. The cost, fuel consumption, is compared with conventional droop control.

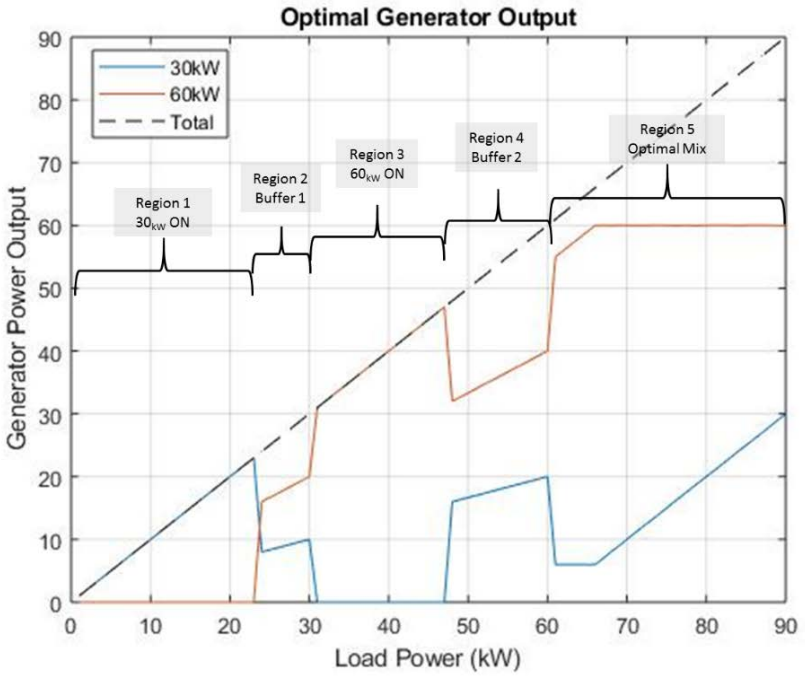

Figure 11. Generator Outputs with Optimization

Table 1. Optimal Dispatch Regions

Region 1	0 kW < P_{load} < 24kW	30 kW ON, 60 kW OFF
Region 2	24kW < P_{load} < 30 kW	30 kW ON, 60 kW ON
Region 3	30 kW < P_{load} < 48kW	30 kW OFF, 60 kW ON
Region 4	48kW < P_{load} < 60 kW	30 kW ON, 60 kW ON
Region 5	60 kW < P_{load} < 90kW	30 kW ON, 60 kW ON

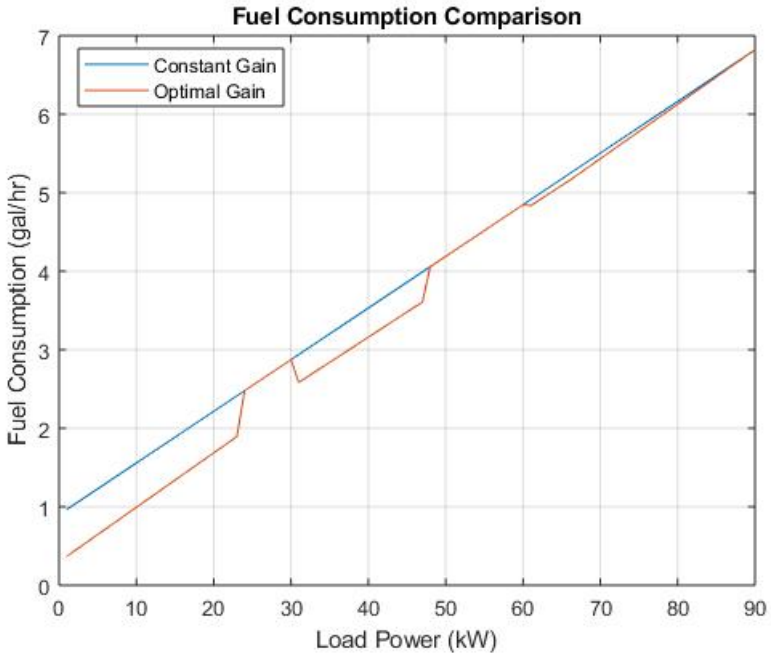

Figure 12. Comparison of Fuel Consumption Rates across Load Spectrum

The optimal gain droop control is either less costly or equivalent to constant gain (conventional) droop. The regions where the two lines are equivalent correspond to the buffer regions because the control is the same in these regions Figure 13 compares the two lines in Figure 12. The plot is generated by using

$$\%_{saved} = \left(1 - \frac{C_{total,optimal}}{C_{total,conventional}}\right) \cdot 100\% . \tag{17}$$

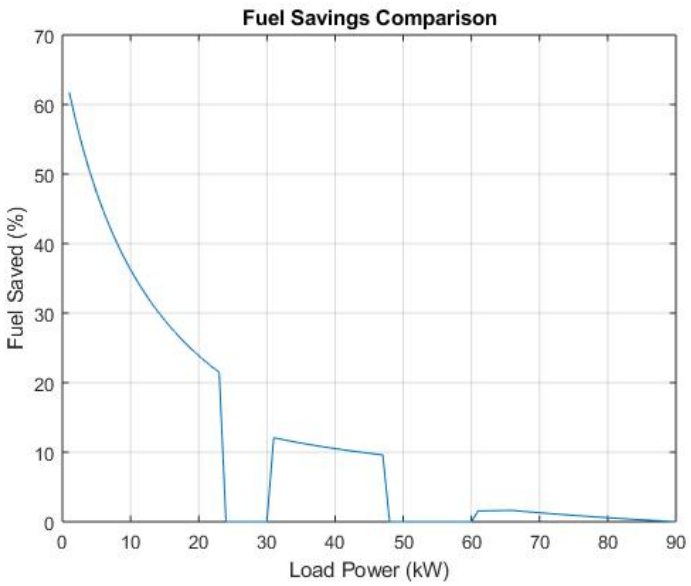

Figure 13. Fuel Savings across Load Spectrum

The majority of fuel savings is achieved for $P_{load} < 60$ kW since both generators have the most efficiency gains for $P_{load} < 0.5P_{rated}$, see Figure 9. For $P_{load} > 60$ kW, the greatest theoretical efficiency gain is 1.6%. This number will vary in reality based on the generators in use and the method to define the cost function. Equation (12) is used to implement the optimal dispatch by creating a virtual resistance for the 60 kW generator, $R_{V,60kW}$, as a function of γ_{opt}. Figure 14 shows the actual droop gains used to implement the optimal control.

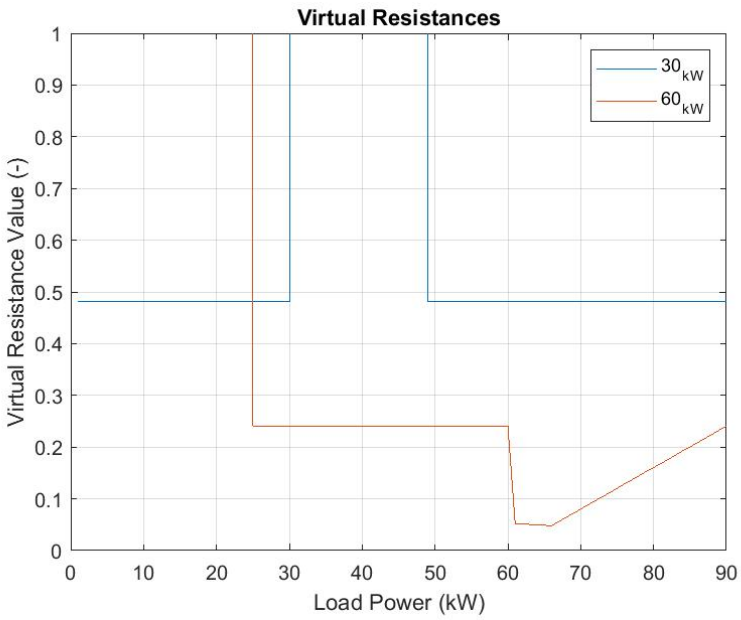

Figure 14. Optimal Virtual Resistance as a function of Load Power

The generator virtual resistances, $R_{V,30kW}$ and $R_{V,60kW}$, are presented for all load values. When the r_V value exceeds '1', its value is set to '1,000' and is high enough to drive the output current for the given generator to zero. In application, this signal would turn the generator off. The plot corresponds to Figure 11 and the regions in Table 1. $R_{V,30kW}$ is constant except when the 60 kW is on only at which point it exceeds 1. Since the power distribution is based on the ratio of the gains, one could theoretically be set at an arbitrary value. $R_{V,30kW}$ was set at its nominal value for constant gain droop. In the last region, $R_{V,60kW}$ is increasing and the physical response is not intuitive. It would appear the 30 kW generator is constant while the 60 kW generator is changing. Figure 14 shows it is the opposite. Again this is due to the values being relative to one another where the reference gain is arbitrary.

C. MICROGRID MODEL

The Simulink model is discussed in a top-down approach starting with a system level view. Figure 15 presents the system view and is comprised of 1) Secondary Controller which affects the system as discussed in Section II; 2) 60 kW Generator and 3) 30 kW Generator containing primary controllers and generator dynamics model; 4) DC Bus with

the load and optimal virtual resistance function; 5) Energy Consumption, which is used for calculations and is not a physical system component. Physical system and control system parameters are presented in Table 2 and Table 3, respectively.

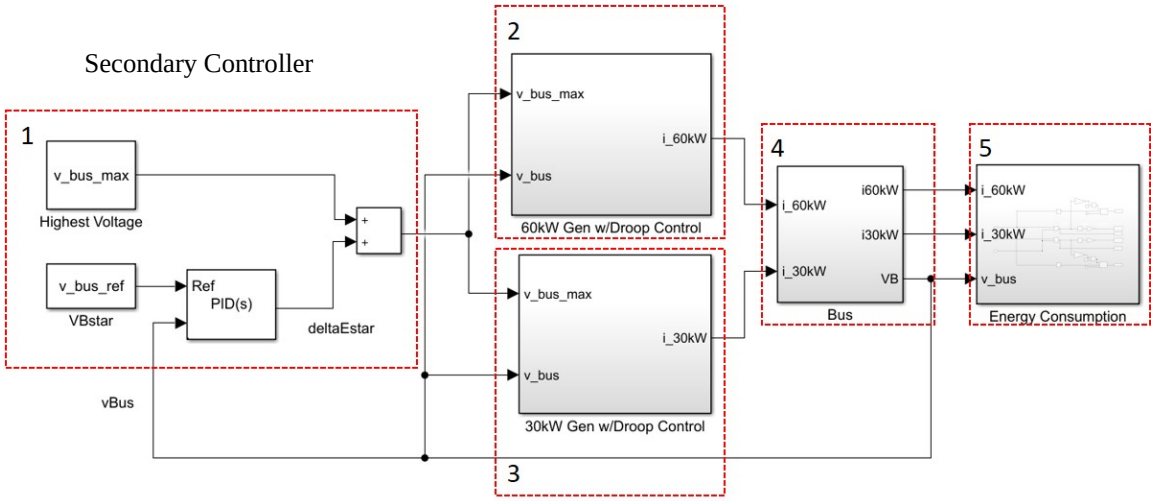

Figure 15. Microgrid Model Overview

Table 2. Physical System Parameters

Variable	Description	Value
$I_{max,30kW}$	30 kW Generator Max Current	78A
$I_{max,60kW}$	60 kW Generator Max Current	157A
$R_{V,30kW,nominal}$	30 kW nominal virtual resistance	0.4813
$R_{V,60kW,nominal}$	60 kW nominal virtual resistance	0.2407
τ_{gen}	Generator time constant	2s
$V_{bus,ref}$	Reference Bus Voltage	380V
$V_{bus,max}$	Max bus voltage	400V
$V_{bus,min}$	Min bus voltage	360V

Table 3. Control System Parameters

Variable	Description	Value
$Kp_{secondary}$	Secondary Controller Proportional Gain	50
$Ki_{secondary}$	Secondary Controller Integral Gain	0.01
$Kp_{primary,30kW}$	30 kW Primary Controller Proportional Gain	1.15
$Ki_{primary,30kW}$	30 kW Primary Controller Integral Gain	1.61
$Kp_{primary,60kW}$	60 kW Primary Controller Proportional Gain	2.31
$Ki_{primary,60kW}$	60 kW Primary Controller Integral Gain	3.23

Only the 60 kW generator, shown in Figure 16, will be viewed to discuss the generator and primary controller model, as the layout is virtually the same for the 30 kW generator.

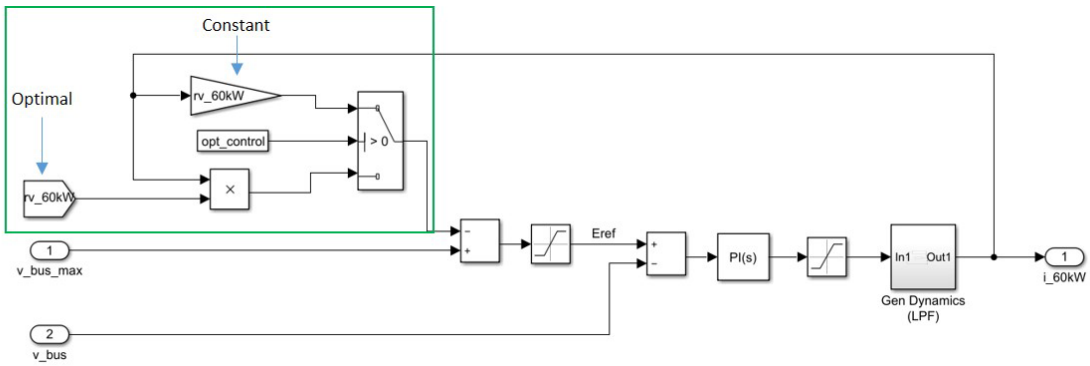

Figure 16. 60 kW Generator and Primary Controller

The generator dynamics are modeled with a first order low pass filter (LPF), which simulates the time delay for the generator output to reach the commanded current level. The control is implemented using (8) from Section II. The model control strategy eliminates the current regulator as the relevant data is simulated for a 24-hr period. The time constant for the current control is small enough to consider the commanded current as the actual current. The key component of the generator and primary controller is highlighted in green in Figure 16. The novel control strategy is implemented in this box. A

selector switch is utilized to compare the constant gain droop control against the variable gain droop control. The variable gain is fed from a separate system block that will be discussed later but is based on the optimal gain value using the previous time-step load power. As can be seen, this method allows for a modular control scheme that replaces only one component in the overall control strategy.

The bus is discussed next which consists of the current summation, load, and optimal droop gain look up table. Figure 17 diagrams the bus as coded in Simulink and Figure 18 shows the model of the load. The bus voltage, $V_{bus,}$ is calculated using (11), where $I = i_{30kW} + i_{60kW}$. The load resistance is determined using a look up table, indicated in Figure 17, and is a function of time.

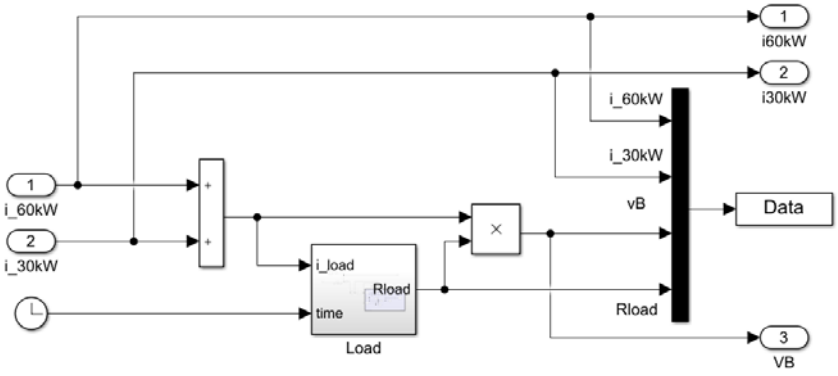

Figure 17. Bus Model

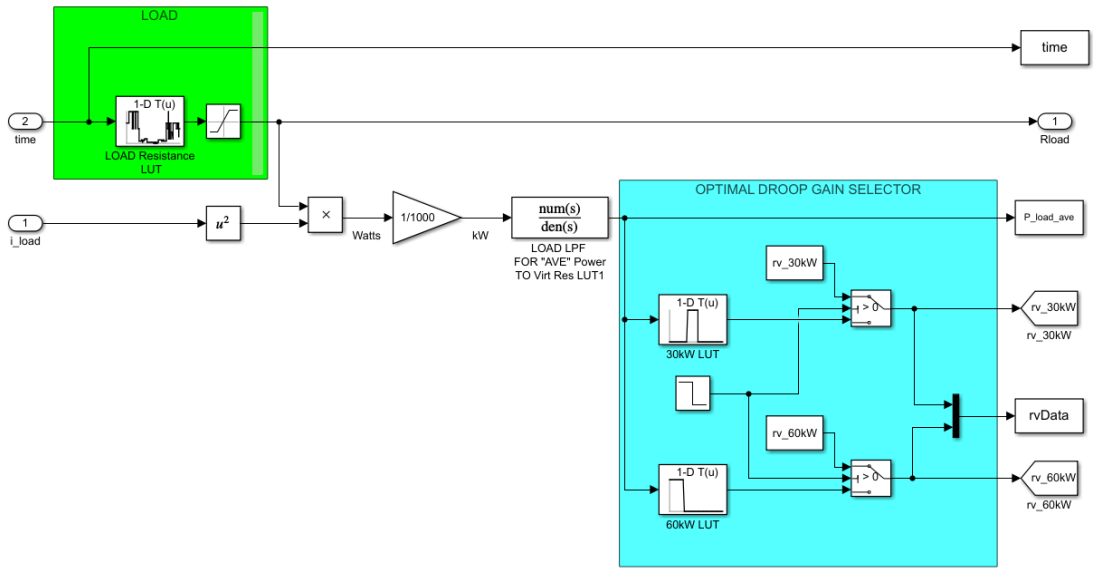

Figure 18. Load and Optimal Gain Selector

The load look up table has a discrete value of the load for each value of time. In modeling, the output of the load table is deterministic. The output is decoupled though, allowing it to function as a stochastic input to the system. Simply put, the optimization does not have prior knowledge of the load. The second subsystem depicted in Figure 18 is the optimal gain selector, which is a function of the load. A first order LPF is used to simulate the time delay in data collection and reduce overly dynamic changes in the variable droop gain. The output is the input to the look up table for each generator. The look up tables were created using the optimization algorithm discussed before. A step input allows the conventional gains to be used in initial simulation to reduce start up transients. As stated before, there is a discrete optimal gain value for each generator at a given load requirement. The variable gains r‘$_{v30kW}$ and r’$_{v60kW}$ are routed to the primary controllers shown in Figure 15.

The currents and bus voltage from Figure 17 are fed to the Energy Consumption block to calculate power, energy, and fuel consumption. Figure 19 implements (3), (5), and (16). When $P_i = 0$, (16) contains a non-zero term for fuel consumption as it is a linear equation with a y-axis intercept. A switch is implemented to prevent this altering the consumption calculations. When $i_i = 0$, the switch outputs a consumption rate $C(P_{load})_i = 0$.

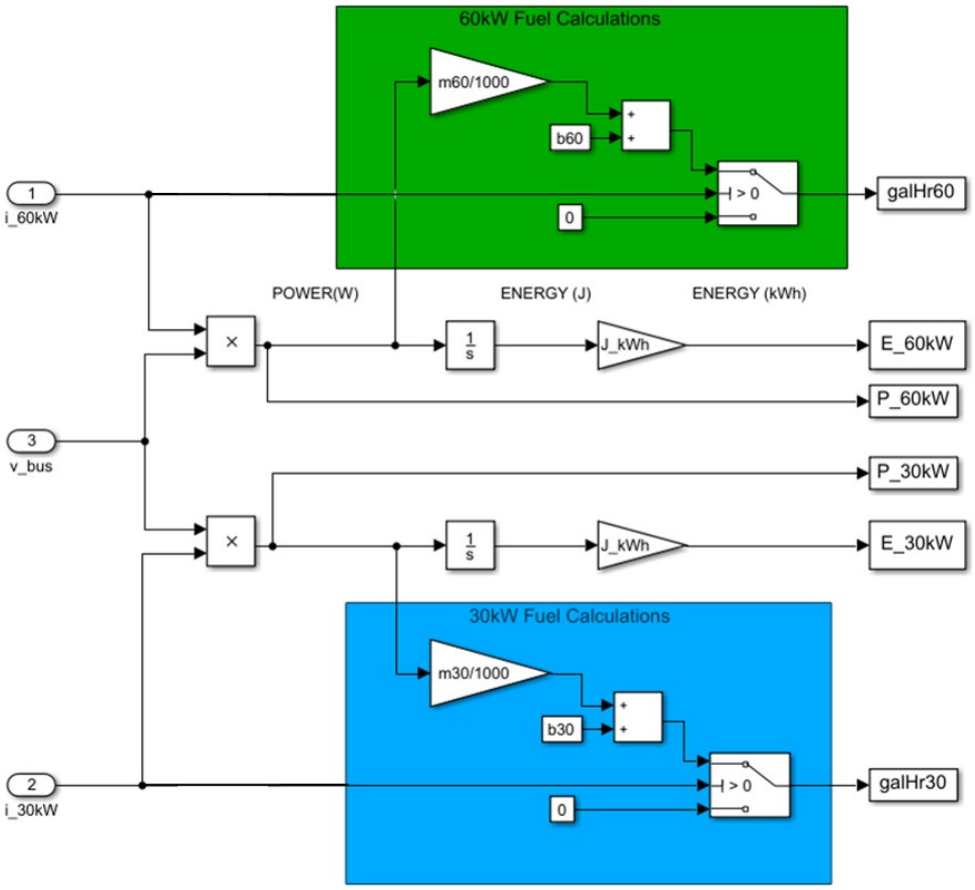

Figure 19. Power and Fuel Consumption Calculation

THIS PAGE INTENTIONALLY LEFT BLANK

IV. RESULTS

Results are compared for conventional droop control and an optimal gain droop control over a 24-hr period. The performance parameters compared were the bus voltage deviation and the fuel efficiency. Other system outputs such as currents and droop gain values will be compared to shown the system operations; each performance comparison will present conventional droop then optimal droop results. The load profile used represents normal operations where demand increases from morning to mid-day then decreases until nightfall. Figure 20 shows the profile used for the simulation. Although the system has a nominal 90 kW capacity, the maximum load requirement is kept below this capacity as practical systems operate with a buffer for potential load spikes. The generator output power and bus voltage are shown in Figure 21 and Figure 22, respectively.

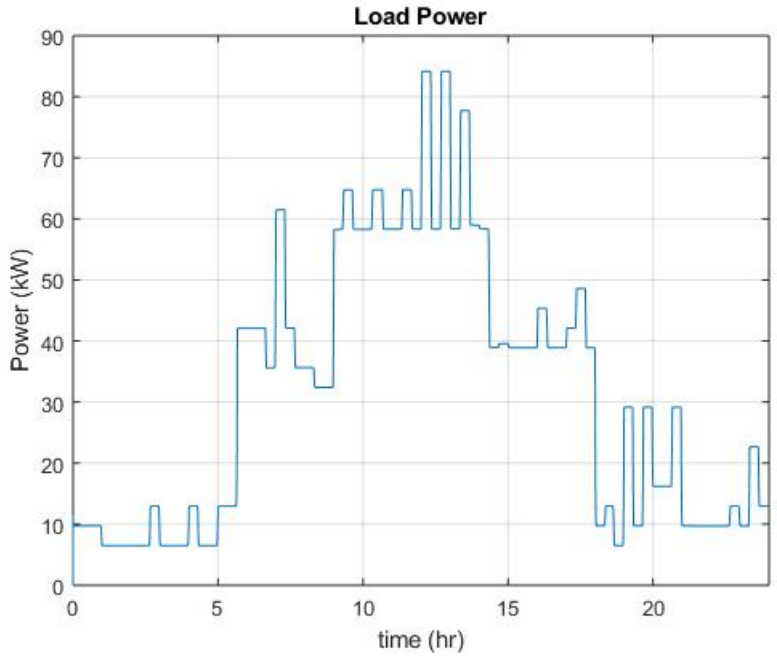

Figure 20. 24-hr Load Profile

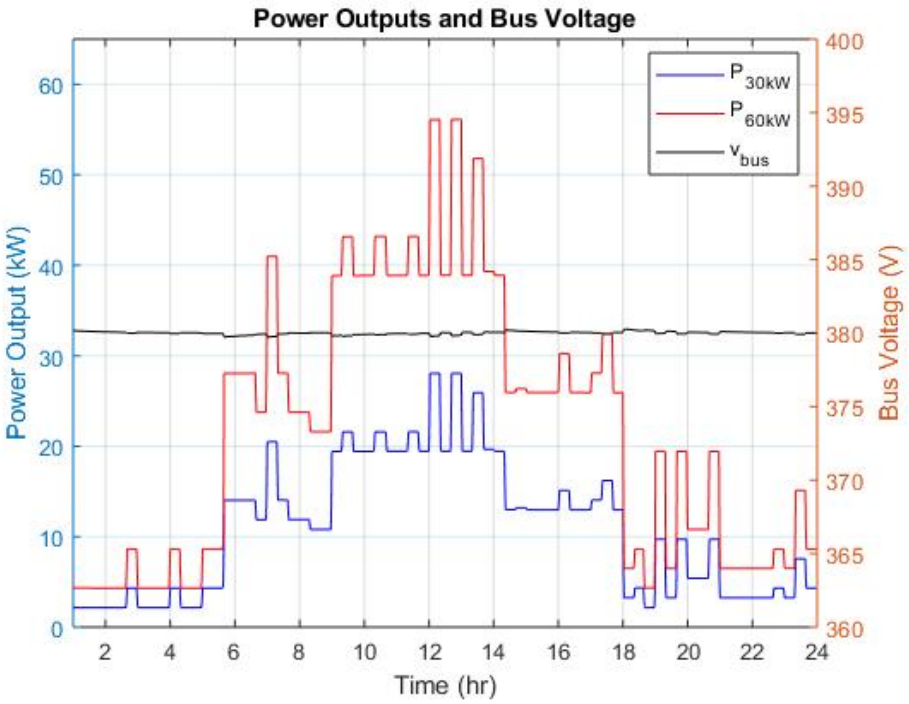

Figure 21. Generator Power and Bus Voltage for Constant Gain Simulation

Observing Figure 21, it is clear that each generator provides a proportional quantity of the load requirement based on its size. For this configuration, the ratio is 2:1, where the 60 kW generator carries 2/3 of the load and the 30 kW carries 1/3 of the load. The bus voltage is displayed from 360V-400V to represent the +/-5% tolerance allowed. The bus voltage does not approach this limit and will be shown in greater detail later.

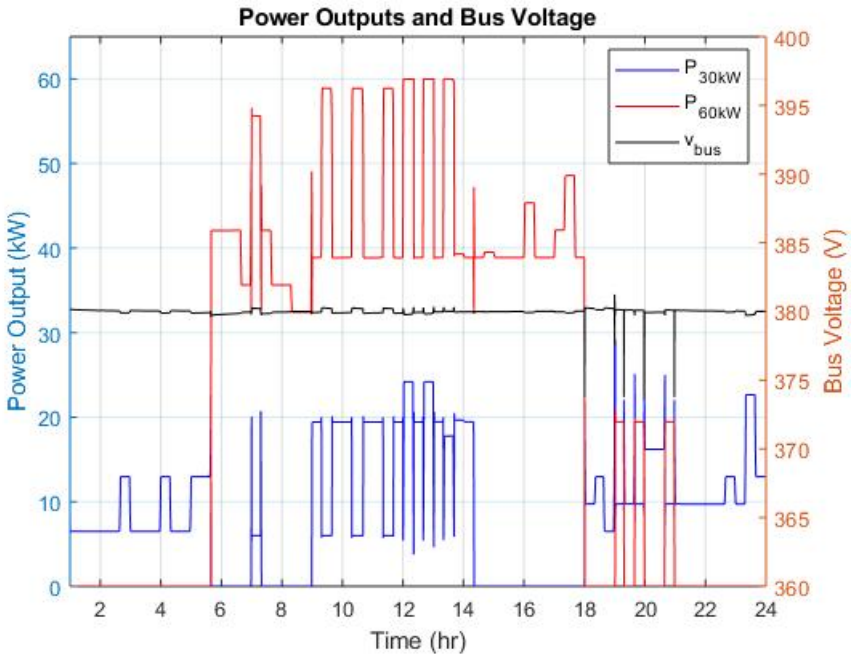

Figure 22. Generator Power and Bus Voltage for Optimal Gain Simulation

Figure 22 shows that with the optimized controller, each generator does not maintain a constant proportion of the load power. The bus voltage is a larger voltage ripple than in Figure 21, but still remains inside the 5% envelope. Figure 23 and Figure 24 show the voltage deviations up close. As stated, the optimal gain bus voltage deviates more frequently at a higher magnitude but never exceeds a 2% deviation, meeting the criteria in [16]. The difference is due to the variable nature of the proposed control law and the transients occurring between buffer regions.

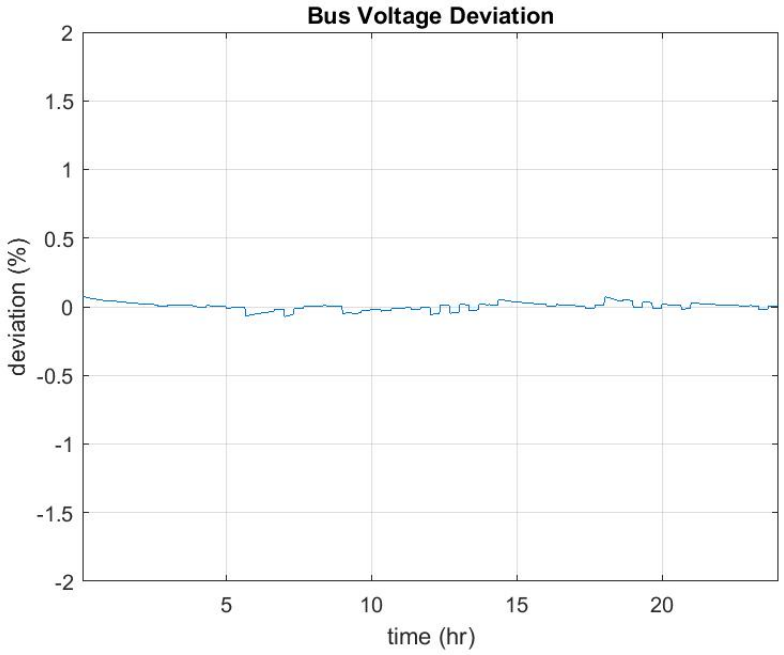

Figure 23. Constant Gain Bus Voltage Deviation

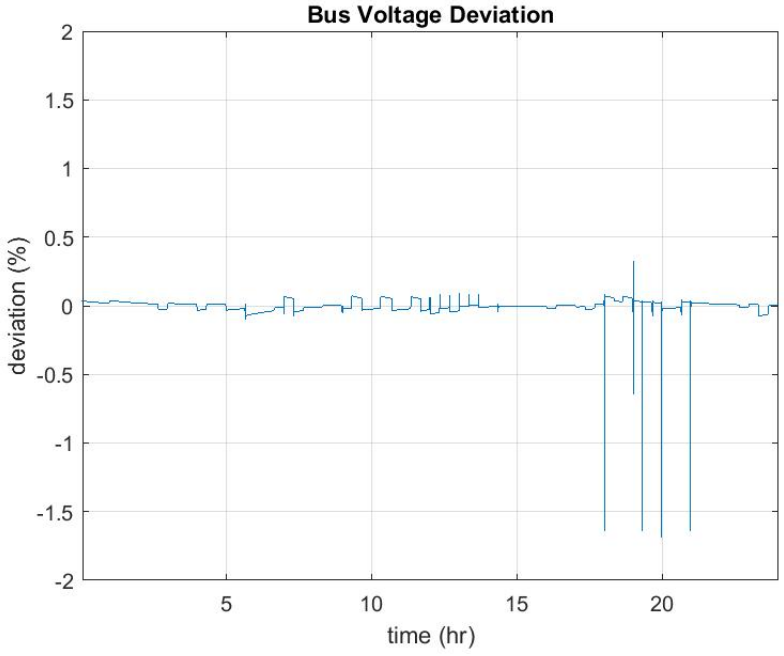

Figure 24. Optimal Gain Bus Voltage Deviation

Figure 25 shows how the optimal gain is implemented during the simulation. The values shown are the real time values for the given load profile based on the virtual resistances shown in Figure 14. The highly variable behavior discussed above can be seen near the end of the simulation when the 60 kW generator experience four shut downs between 18 and 21 hours. During this window, the load does not exceed 30 kW and the 'buffer regions' actually cause the fluctuation. The minimum time between an on/off event was 18 minutes, which is also within acceptable limits from [16].

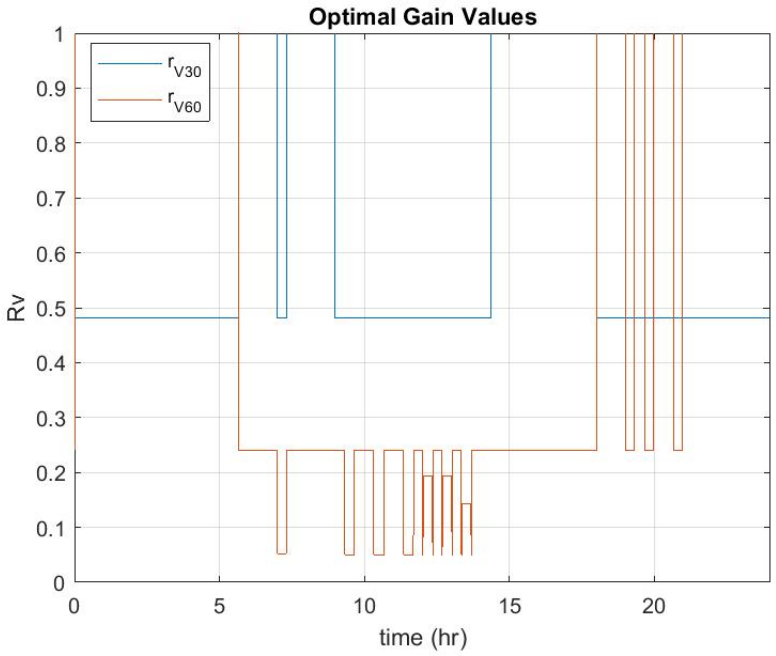

Figure 25. Virtual Resistances for Optimal Droop

With the bus voltage criteria met, the fuel efficiency will now be analyzed. Figure 26 and Figure 27 show the fuel consumption for the constant gain droop control and optimal gain, respectively.

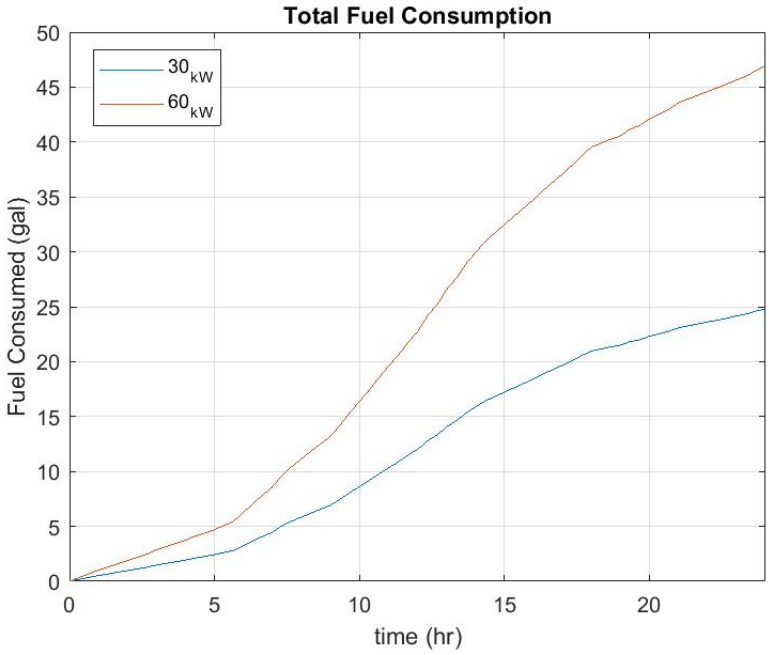

Figure 26. Cumulative Fuel Consumption for Constant Gain Simulation

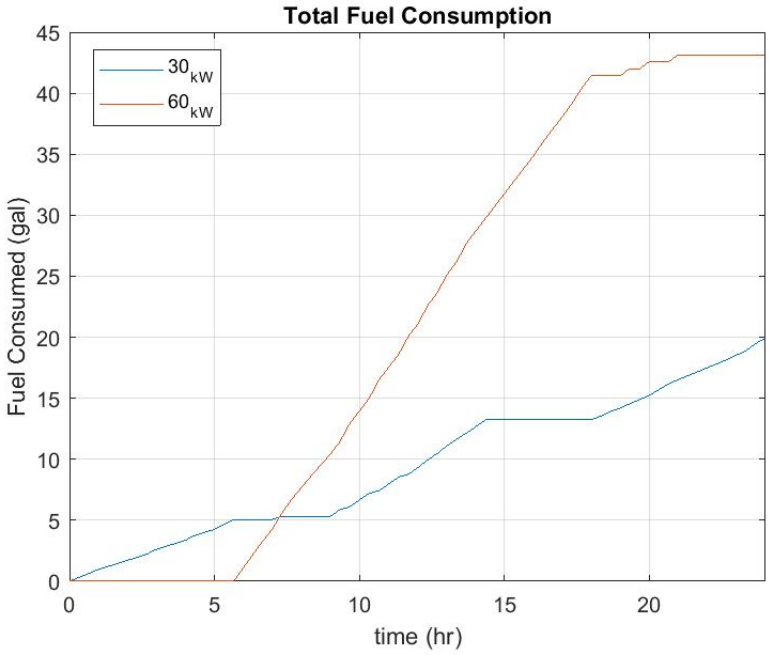

Figure 27. Cumulative Fuel Consumption for Optimal Gain Simulation

The constant gain simulation has continuously increasing fuel consumption while the optimal simulation contains plateaus where a generator has been turned off. The proposed control law increases the configuration efficiency by 12.06% for this load profile. Different load profiles will gain varying degrees of efficiency but will not have lower efficiency than one with constant gain droop control. Table 4 displays the efficiency comparison for conventional droop and optimal droop control.

Table 4. Fuel Comparison (Constant vs. Optimal)

Control Law	**Fuel**	**Units**
Constant Gain	71.64	gal
Optimal Gain	62.99	gal
Percent Saved	12.06%	

THIS PAGE INTENTIONALLY LEFT BLANK

V. EXPERIMENTATION

A. INTRODUCTION

The modeling and simulation presented focuses on two key concepts for increasing generator efficiency: optimal generator selection and optimal dispatch of power. The optimization approaches discussed were implemented on three-phase AC generators operating in the different optimization modes. Experimentation was conducted in collaboration with the Massachusetts Institute of Technology, Lincoln Labs Energy Team using their tactical power test bed. Experimentation analyzed the performance of the generators in four distinct operating modes:

1. Conventional Droop
2. Droop with Optimal Generator Selection
3. Variable Droop Slope for Frequency
4. Variable Droop Line Offset for Frequency

Conventional Droop consists of two generators in parallel, both carrying the load based on their rated capacity. Droop with optimal generator selection operates the same as conventional droop with the addition of turning a generator on or off based on the most fuel-efficient configuration. “Variable droop slope for frequency” changes the slope of the droop line, shown in Figure 28. “Variable droop line offset for frequency” changes the y-intercept for the droop line, shown in Figure 29. Voltage and current data was collected for each generator and processed to generate frequency and power data. All tests used a resistive load bank with a small inductive load from the cooling fan. Load changes occurred manually at discrete levels with physical switches.

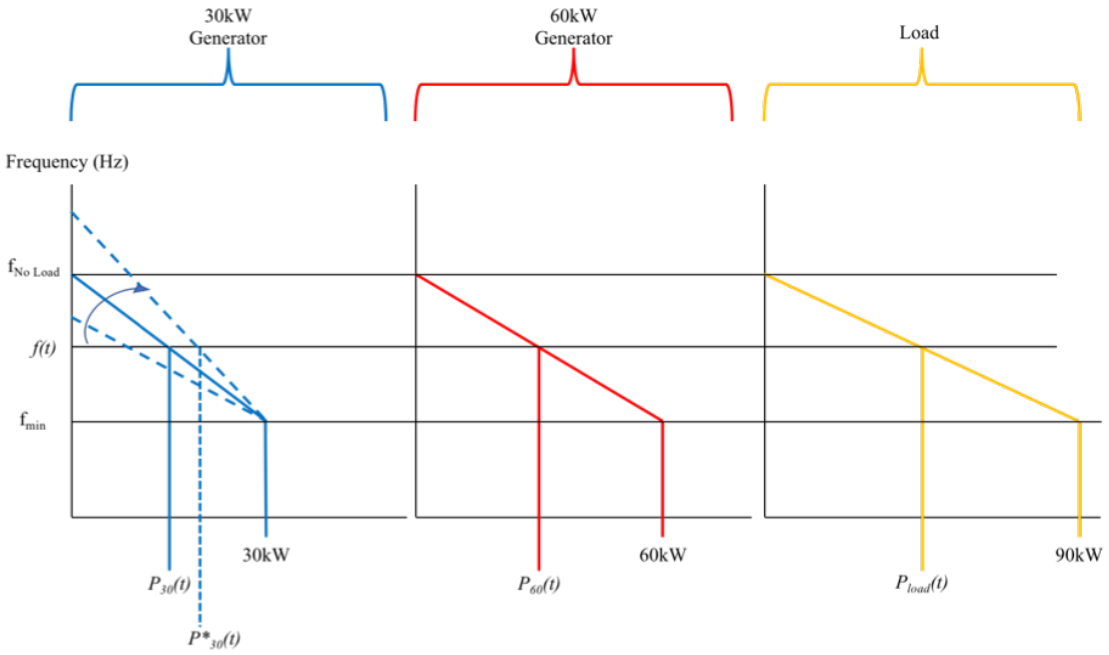

Figure 28. Droop Lines with Variable Frequency Droop Slope

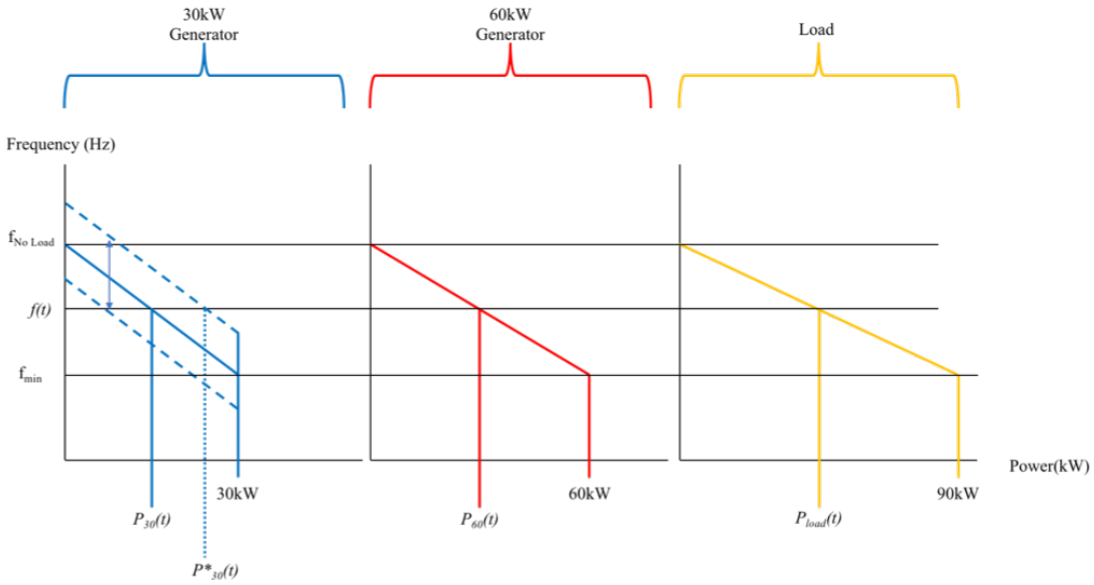

Figure 29. Droop Lines with Variable Frequency Offset

In Section 2, Figure 4 displays the droop line for a DC system. An AC system uses frequency in place of voltage (y-axis) and power in place of the current (x-axis). Voltage is used to control reactive power in an AC system, which will not be discussed in this thesis. The parameter changes shown in Figure 28 and Figure 29 have the effect of altering the power distribution. The load requires a certain frequency to produce the required load power. Each generator will settle on this frequency via a primary control loop that moves the frequency along the set droop line. Changing the line changes the intersection of frequency and power. Holding one generator droop line constant allows the ratio to be skewed from its nominal value. Since the 60 kW generator is twice the rated size of the 30 kW generator, the nominal ratio is 2:1 where the 60 kW generator carries 2/3 of the load and the 30 kW generator carries 1/3 of the load. Increasing the slope or frequency offset results in more load demand on the given generator, if the other generator keeps constant parameters. Decreasing the slope or frequency offset reduces the load demand on the given generator. With the optimization mapped from a DC microgrid to an AC microgrid, the test scenarios are implemented and analyzed.

B. TESTS AND RESULTS

1. Test 1 Procedure: Conventional Droop

Test 1 consists of the 30 kW and 60 kW generator operating in parallel with droop mode. Both generators operate for the duration of the test and run for thirty minutes under a comparable load presented in Figure 20. With both generators running in droop mode and the load bank connected to the bus, the load was changed to a set magnitude at a set time. A sample of this procedure is shown in Table 5.

Table 5. Test 1 Procedure Sample

state	time		Load	30kW State	60kW State	Load Switches					
#	min	s	kW	#	#	3.75	7.5	7.5	18.75	37.5	75
1	0	0	9.72	1	1	1	0	0	1	0	0
2	1	10	6.48	1	1	1	1	0	0	0	0
3	3	10	12.96	1	1	1	1	0	1	0	0
4	3	34	6.48	1	1	1	1	0	0	0	0
. . .	. . .	. . .	. . .	. . .	. . .	. . .	. . .	. . .	. . .	. . .	. . .

2. Test 1 Results

Figure 30 shows the power for each generator and the total load. The load is distributed based on a 2:1 ratio and each generator transient response is proportional to its rating.

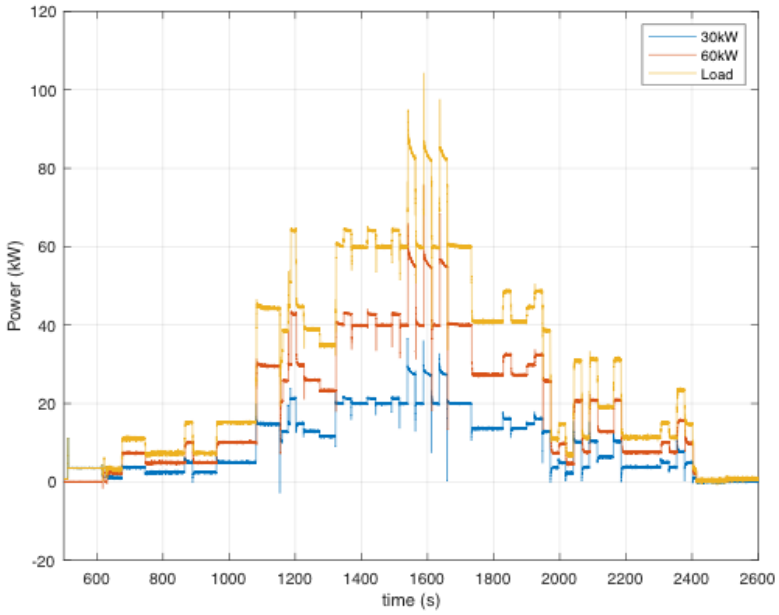

Figure 30. Power, Conventional Droop

The transient behavior shown in Figure 30 for power translates to transients in the frequency. Since the frequency increases and decreases along the droop lines, the steady state value is also influenced. Figure 31 displays the frequency changes over time.

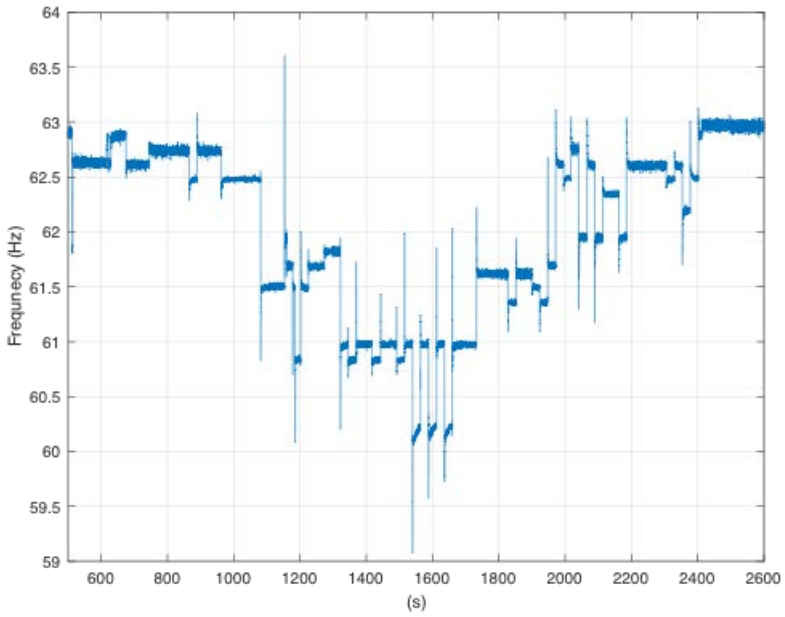

Figure 31. Conventional Droop Frequency vs. Time

Changes in the load result in proportional spikes in the frequency. The generators tested use a 63–60 Hz droop line. This control method allows the frequency to settle on values other than 60Hz. MIL STD 1332B [16] allows for +/-5% regulation of the frequency using a 60Hz reference. Frequency regulation stays within these specifications. The steady frequency correlates directly with each generator droop line which is presented in Figure 28. Figure 32 and Figure 33 show the frequency vs. power data. Although the signal noisy, clusters where the steady state frequency settle are clearly seen and the droop line is plotted on top of the data to show the correlation.

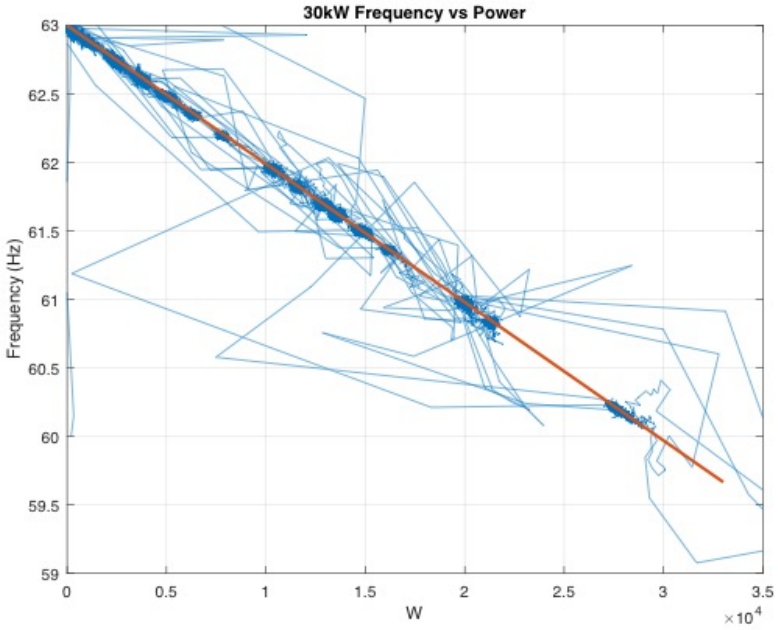

Figure 32. 30 kW Experimental Droop Line

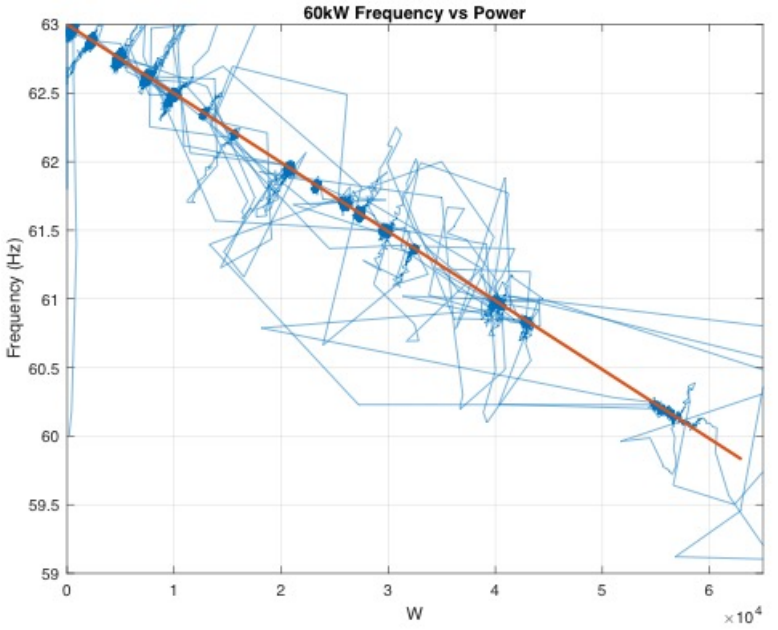

Figure 33. 60 kW Experimental Droop Line

Figure 34 presents the root-mean squared (RMS) voltage and current for the bus and individual generators on a single phase. Larger loads result in greater current demand, frequency drop, and voltage drops. Voltage spikes can be seen as a large load is shed. [16] allows for a 15% voltage dip or spike which yields a $102V_{rms}$ – $138V_{rms}$ tolerance. The voltage regulation has a maximum transient of 8.5%, staying within limits.

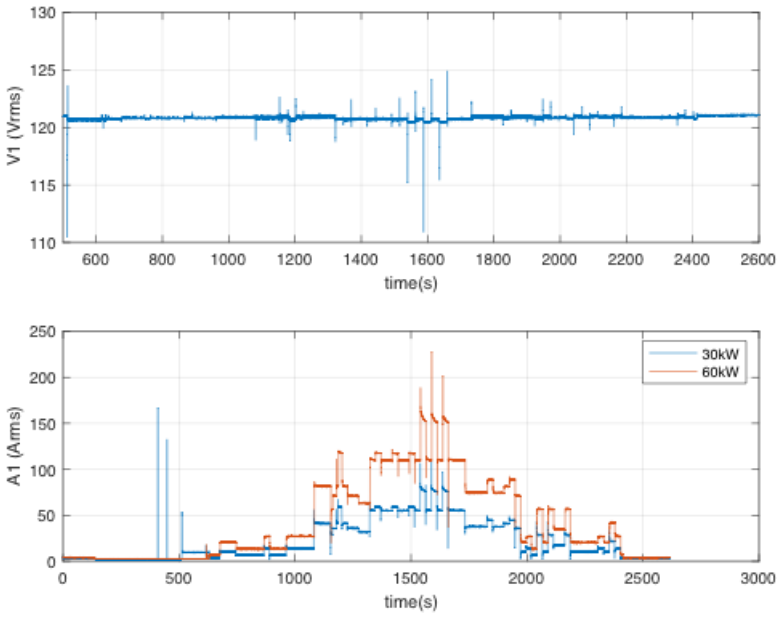

Figure 34. RMS Voltage and Current

3. Test 2 Procedure: Optimal Generator Selection

Test 2 is conducted the same as Test 1 with the addition of generators turning off and on. The optimal configuration was established manually with one person physically turning a generator on or off. Each change of state required the load to change first, then the generator state would change. If both generator states were changing (30 kW-HIGH, 60 kW-LOW → 30 kW-LOW, 60 kW-HIGH), the load would be applied, followed by turning on both generators, then shedding the unneeded generator. This procedure is sampled in Table 6 and highlighted for states 2–3.

Table 6. Test 2 Procedure Sample

state	time		Load	30kW State	60kW State	Load Switches (kW)					
#	min	s	kW	#	#	3.75	7.5	7.5	18.75	37.5	75
1	3	34	6.47	1	0		1	0	0	0	0
2	4	46	13.97	1	0		1	0	1	0	0
3	6	46	43.64	1	1		1	0	0	0	1
4	-	-	43.64	0	1		1	0	0	0	1
5	7	58	37.59	0	1		0	1	1	1	0
6	8	22	63.24	1	1		1	0	0	1	1

4. Test 2 Results

The Test 2 load profile is the same as Test 1 with some redundant events removed. Figure 35 shows the power for each generator and the load. Periods where the power for a generator is zero corresponds with the generator turning off. When both generators are on, they share power based on their rated capacity; 2:1 ratio. Figure 36 shows the frequency over time. Comparing with Figure 30 from Test 1 shows the steady state frequency is a function of the load power, not the number of generators running. The generator states only influence the severity of the transients.

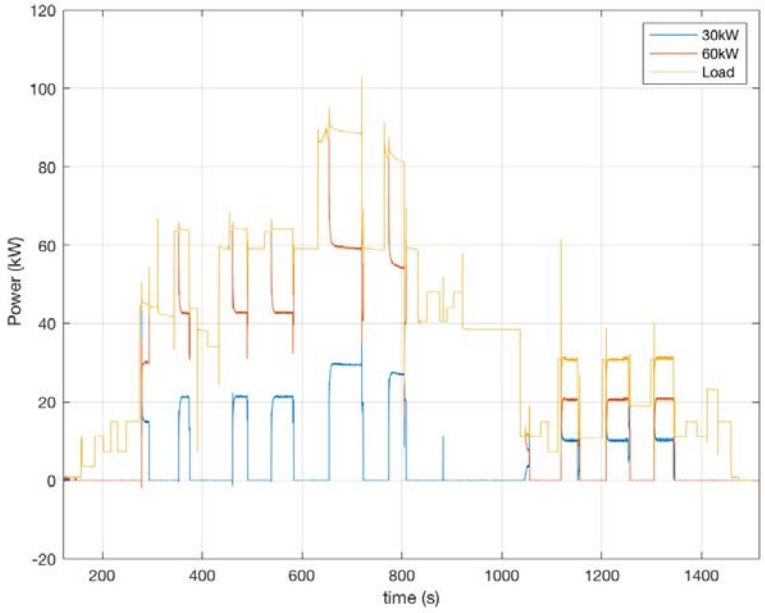

Figure 35. Power, Droop with Optimal Generator Selection

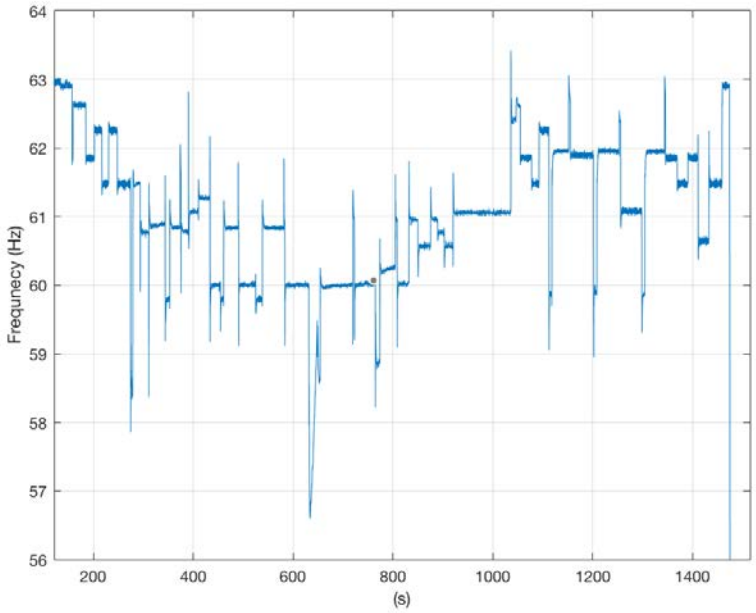

Figure 36. Frequency vs. Time for Optimal Generator Selection

Figure 37 displays the RMS voltage and current and provides two key observations. First, the voltage transients are larger in magnitude and occur more frequently than the case shown in Figure 34, where both generators remain on. The largest voltage transient is 10.8% of the rated voltage, 2.3% higher than conventional droop. The frequency and voltage are controlled using different control loops and command signals, but Figure 36 and Figure 37show the two respond proportionally to system perturbation. The second observation relates to the current transients. Contrary to the higher transient behavior seen in the voltage and frequency, the current transients are less severe in the optimal generator selection case. This could be attributed to a reduced impedance with parallel generators and increased inertia. The greater inertia and smaller resistance to current when both generators are on means a greater current response when the load changes.

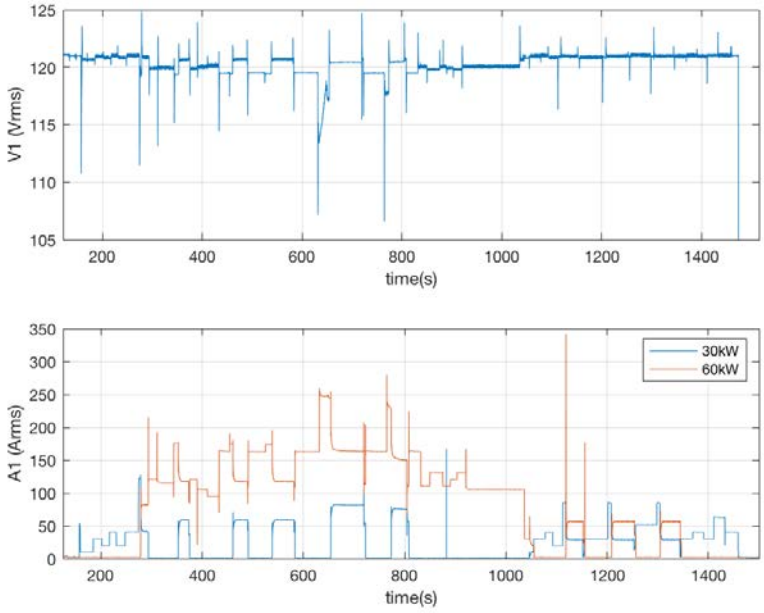

Figure 37. RMS Voltage and Current for Optimal Generator Selection

5. Test 3: Variable Frequency Droop Line Offset

The goal for Test 3 was to evaluate the performance of each generator when the offset of the droop line is changed as shown in Figure 29. The procedure was conducted in four steps.

1. Increase 30 kW Frequency Droop Line Offset (1Hz Increments)
2. Decrease 30 kW Frequency Droop Line Offset (1Hz Increments)
3. Reset to Default Droop Offset
4. Decrease 30 kW Frequency Droop Line Offset
5. Increase Load and 30 kW Frequency Droop Line Offset

Steps 1–3 kept a constant load of 60 kW while the offset was changed. Step 4 changed the load and the offset sequentially. All changes in load and offset were done manually by testers.

6. Test 3 Results

Test 3 and 4 introduce 2–3 changing variables in the load, droop line slope, and droop line offset or y-intercept. The power plots, Figure 38 and Figure 45 provide a reference for what types of changes occur. If the load stays constant for a given change, the adjustment occurred to the slope or offset. All load changes occur without any other adjustments. Adjustments are done after the load change.

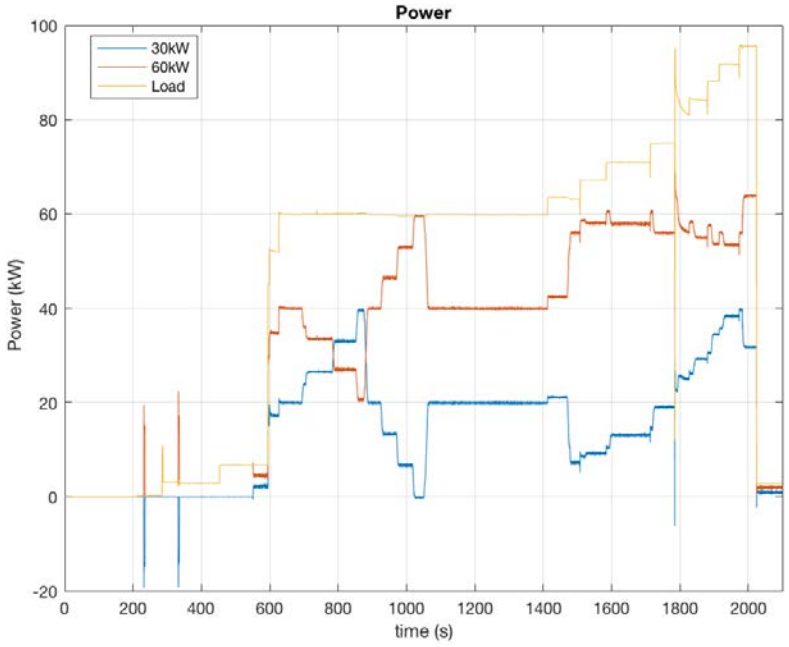

Figure 38. Power for Variable Frequency Droop Offset

Figure 39 provides a clearer picture of how the changing parameters compare to the conventional droop with respect to power distribution. The red dashed line shows the default percentage of power a generator carries in conventional droop. The 30 kW generator frequency offset was adjusted while the 60 kW generator kept constant values. This results in inverse behavior on the 60 kW when the 30 kW is adjusted. For cases where the 30 kW percent loading exceeds the red line, the offset was increased. When the 30 kW loading is below the red line, the offset was decreased.

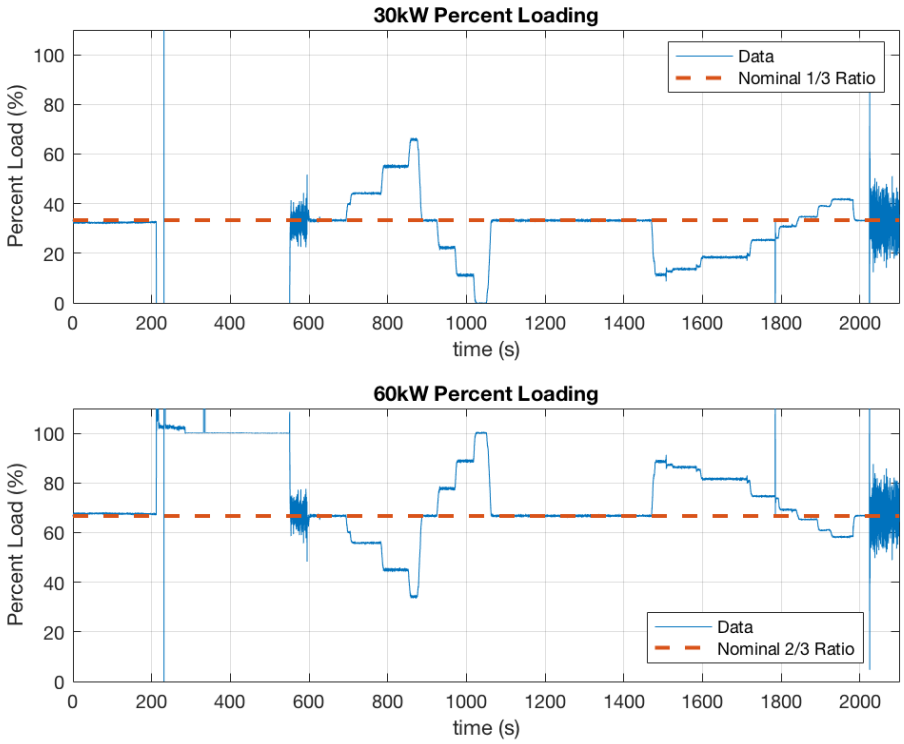

Figure 39. Percent Loading for Variable Frequency Droop Offset

From Figure 29, the frequency is initially set by the load and the slope of the load's droop line. If the droop lines for the other generators remain constant, this frequency set point holds true. Changing the frequency offset for the 30 kW generator influences the steady state frequency on the bus. Since the 30 kW generator carries more load or less load than the default line, the 60 kW generator will carry less or more load as well. The new steady state frequency satisfies both droop lines. When the load is increased, the 60 kW generator can maintain a relatively constant output while the 30 kW generator increases its output. This results in less deviation in the steady state frequency but greater transients seen between 1500s and 2000s.

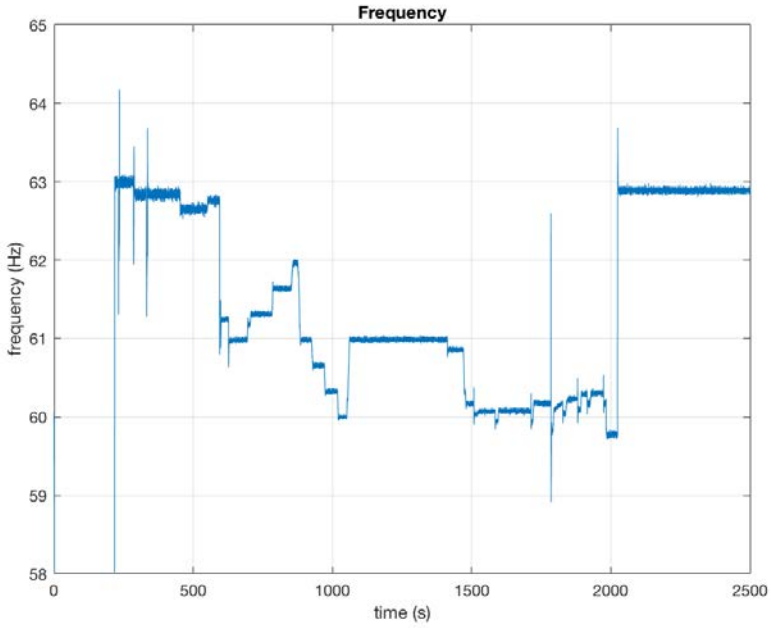

Figure 40. Frequency for Variable Frequency Droop Offset

Figure 41 shows the experimental data represented by Figure 29. Changes in the offset produce data points that fall precisely along new droop lines. Integer values for frequency offset changes are presented, but data clusters between correlate to 0.1Hz changes in the frequency offset. The lines are labeled “FA” for frequency adjust. Data points between the lines show the path for the frequency change when the offset was changed.

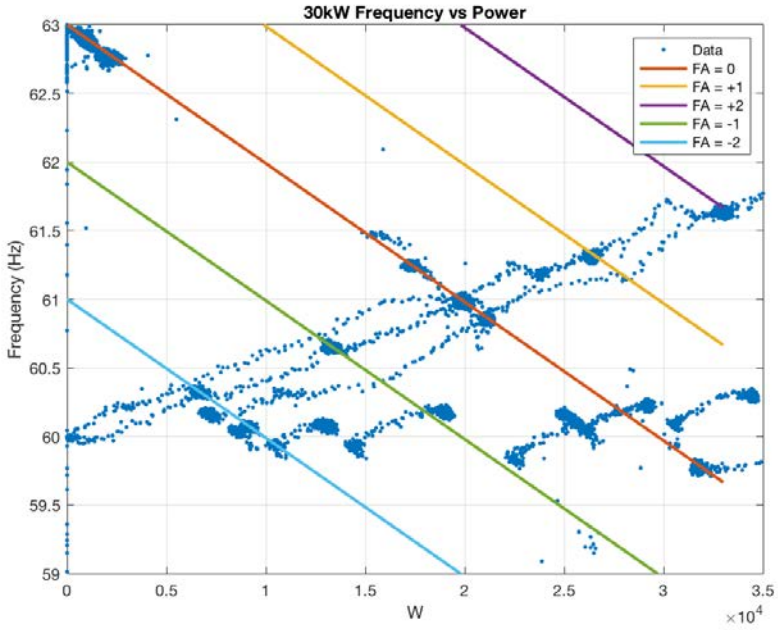

Figure 41. 30 kW Frequency Droop for Variable Frequency Droop Offset

While the 30 kW frequency offset was changed, the 60 kW parameters remained constant. Figure 42 shows the droop line is not influenced by changes in the 30 kW generator. This enables the control of power distribution.

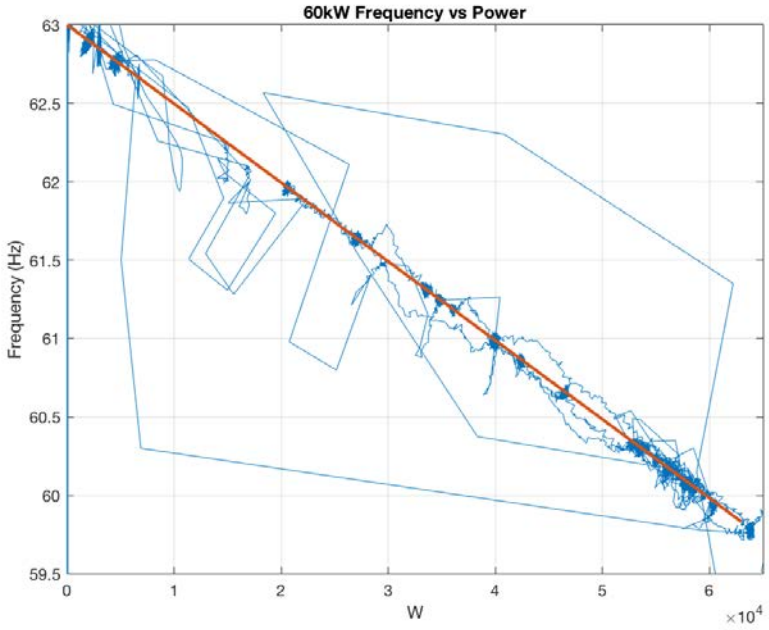

Figure 42. 60 kW Frequency Droop for Variable Frequency Droop Offset

The frequency regulation under changing offsets performed well and maintained outputs within +/-5% in accordance with [16]. During load increases, the voltage transient is less than 5%. Figure 43 shows the RMS voltage and current.

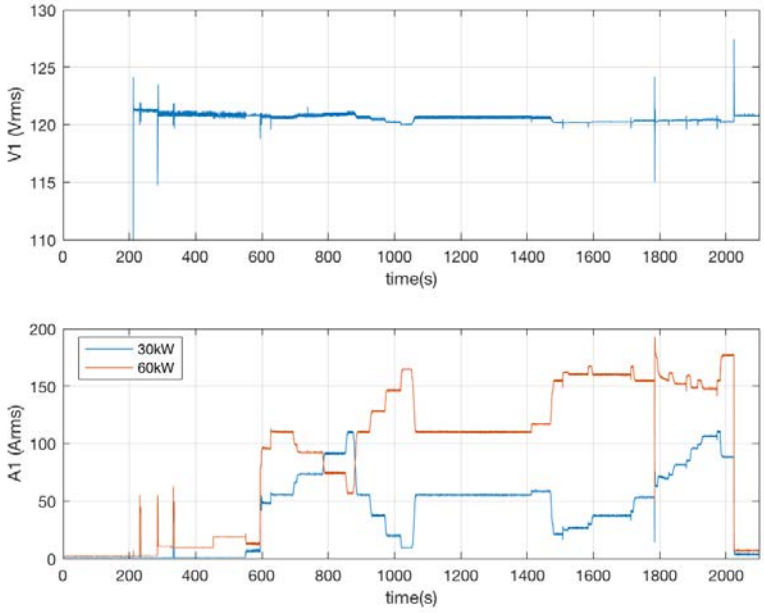

Figure 43. RMS Voltage and Current for Variable Frequency Droop Offset

7. Test 4 Procedure: Variable Frequency Droop Slope

The goal for Test 4 was to evaluate the performance of each generator when the slope of the droop line is changed as shown in Figure 28. The procedure was conducted in four steps.

1. Increase 30 kW Frequency Droop Line Slope: 10%
2. Vary Load
3. Decrease 30 kW Frequency Droop Line Slope: 2%
4. Vary Load

The default slope for both generators is 5%, meaning the change in frequency from 0kW to P_{max} is 5% of 60Hz or 3Hz total. Increasing the slope to 10% increases the range to 6Hz while decreasing to 2% decreases the range to 1.2Hz. The generators do saturate near the maximum power levels but will exceed the rated capacity during transients and at steady state. This behavior is seen and discussed in results. To accommodate for saturation, the frequency offset was also adjusted and is shown in Figure 47. Figure 44 shows how the slope increases and decreases using the maximum power as the anchor point.

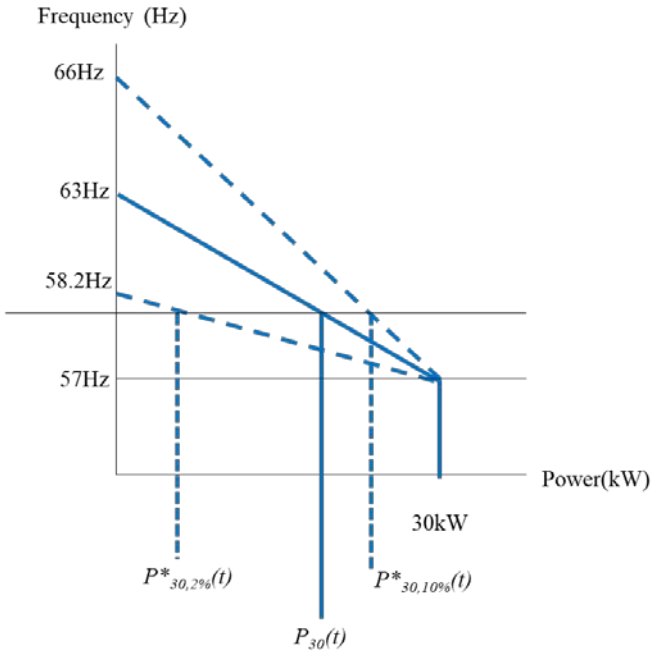

Figure 44. Variable 30 kW Droop Line Slope

8. Test 4 Results

Test 4 changes both slope and offset of the droop line for the 30 kW generator only. The rules for changes from Test 3 apply for Test 4. The load changes first, followed by changes to the droop line. Any changes in the generator output without a change in the load mean the droop line was altered. Additionally, if a given generator output appears to be zero, the generator is still operating. In these cases, the droop parameters are set so the output is near-zero. In Figure 45 and subsequent figures, a high oscillation can be seen between 250s and 500s. This is a result of instability created when changing the droop slope to 10%. Reducing the gain on the control signal that regulates the frequency helped return the system stability. Although the system recovered, it demonstrated the instability created in the system by changing the droop slope.

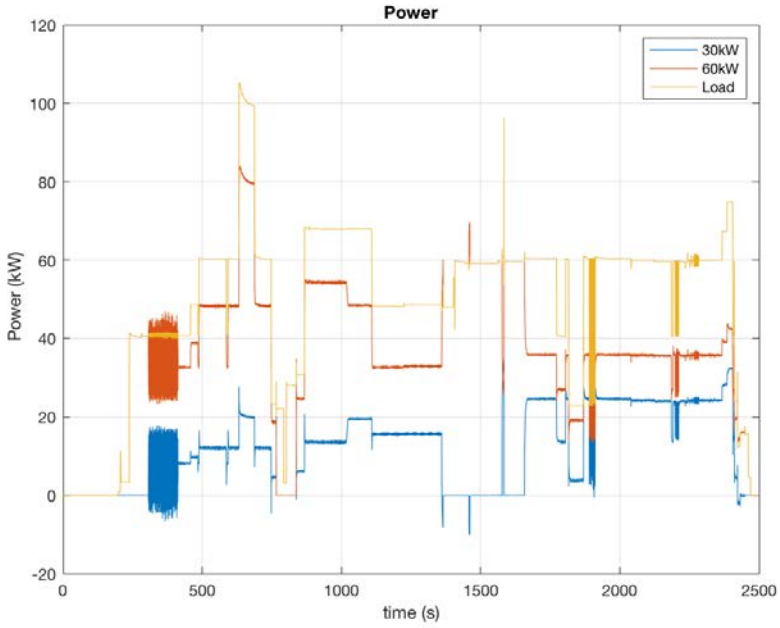

Figure 45. Power for Variable Frequency Droop Slope

The purpose of changing the slope is to control the power distribution between the generators. Figure 46 displays how the power is distributed during the test. The red dashed line shows the default percentage each generator carries without adjusting the slope. From Figure 44 it can be seen that a greater slope results in a greater percentage of power for the given generator. This expected behavior cannot be seen in Figure 46 as the frequency offset was adjusted to help stability and reduce oscillations. When the slope was set at 10%, the frequency offset was decreased and when the slope was set at 2% the frequency offset was increased. These changes are shown in Figure 48.

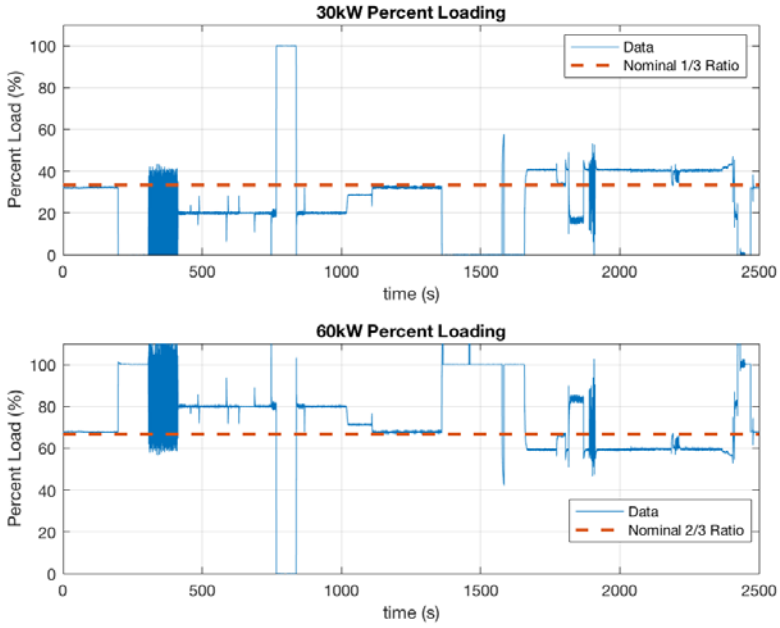

Figure 46. Percent Loading for Variable Frequency Droop Slope

When the slope is changed, the generator will respond more slowly or more quickly than originally designed. This has a multiple layer effect because the generator controls operate on tuned time constants. Changes in the speed of a response may not align with the speed of the other control loops. The problem is amplified when the two generators operate at different slopes. In default settings the generators will respond at proportional speeds, but different slopes create disproportionate responses. These factors adversely affect the frequency, causing more severe transients and less stable steady state behavior. Figure 47 shows this adverse impact to frequency over time.

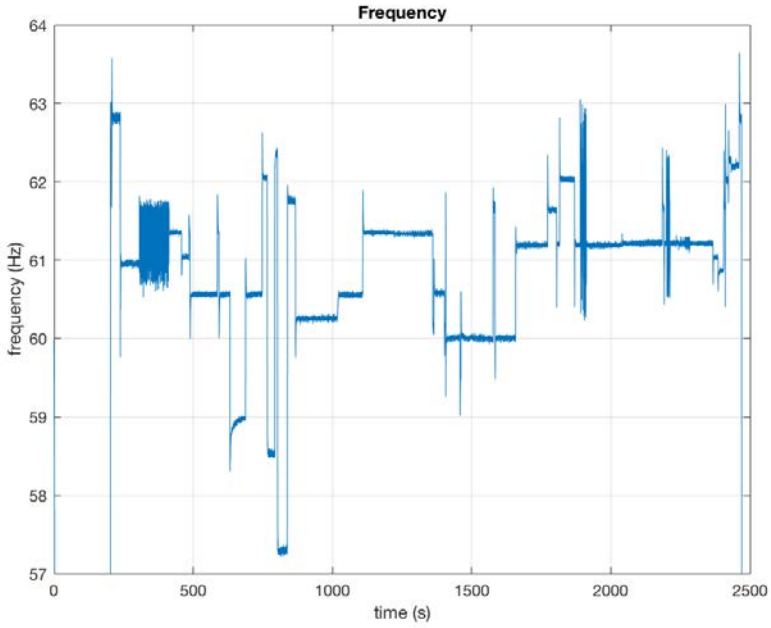

Figure 47. Frequency for Variable Frequency Droop Slope

The changes in slope and offset are shown in Figure 48. If no offsets are used, the droop lines converge at the intersection of 60Hz and 30 kW. This shows the droop slope is defined from P_{max} at 60Hz and aligns with the theory discussed with Figure 28. Without the addition of offsets, the power output of the 30 kW generator easily exceeds its rated capacity.

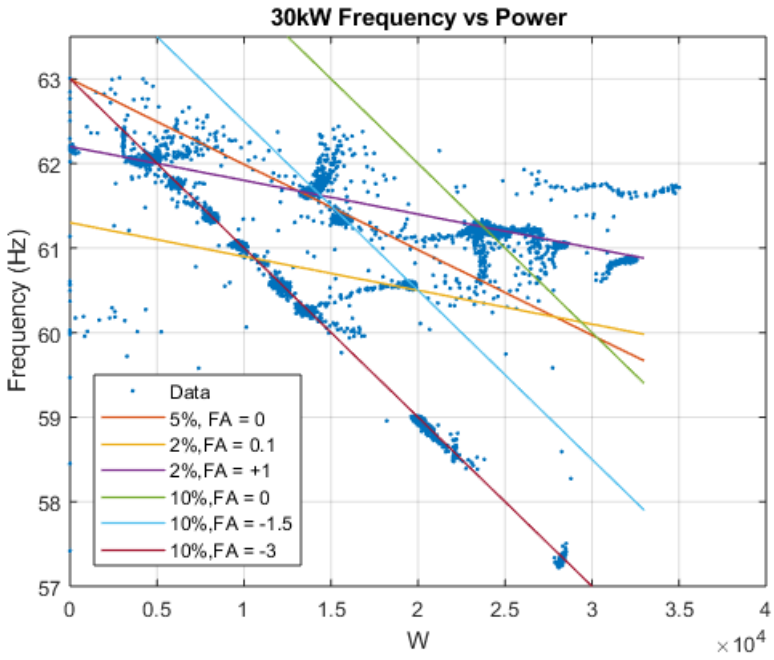

Figure 48. 30 kW Frequency Droop for Variable Frequency Droop Slope

In Figure 49 it can be seen again that changes to the 30 kW generator parameters do not affect the steady state behavior of the 60 kW generator. There are increased oscillations and transients due to the instability introduced by the 30 kW generator, but the frequency always settles along the default droop line. Figure 50 shows the RMS voltage and current with behavior consistent with frequency.

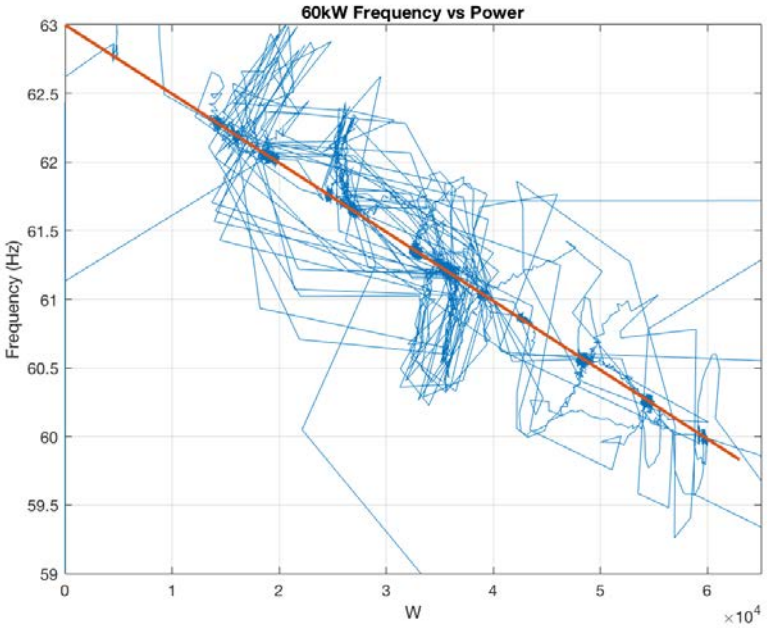

Figure 49. 60 kW Frequency Droop for Variable Frequency Droop Slope

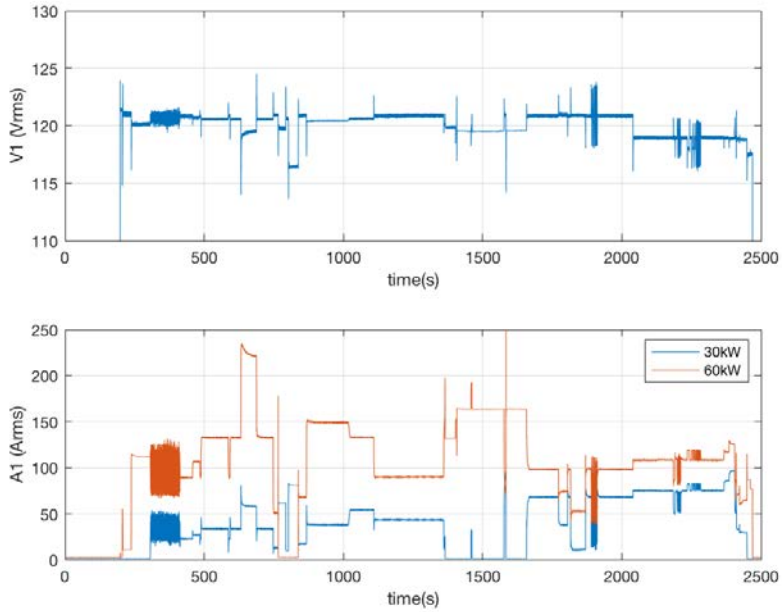

Figure 50. RMS Voltage and Current for Variable Frequency Droop Slope

The four experiments presented tested microgrid performance with respect to voltage and frequency regulation under different load sharing control methods. Conventional droop results in large transients but provides a stable system with high reliability. Optimal Generator Selection reduces current transients but has increased voltage and frequency swings. These transients could be improved by ramping the power up or down when a generator comes online or goes offline. Simply cutting a generator off has the effect of applying a large load which introduces the transient seen. The variable frequency offset method maintained stability and acceptable voltage and frequency deviations even during transients. The load profile was limited and did not fully test the performance under severe load changes. In contrast, the frequency droop line slope changes created a marginally stable system. When the system was stable, the adjusted slope created issues with saturation at the upper and lower bounds of the generator outputs. The frequency offset had to be adjusted to allow the generators to operate properly. Based on the performance of the three optimization methods, the optimal generator selection and variable frequency offset provide viable methods while the variable slope is currently unviable.

VI. CONCLUSIONS AND FUTURE WORK

The primary objective of this thesis was to present a method for controlling military microgrids more efficiently. The proposed method accomplishes a reduction in fuel consumption while still providing the required performance. In addition, the modeling and simulation demonstrated the effect of tuning one variable, the virtual resistance, for each generator. Military microgrid efficiency can be achieved by overlaying a tertiary controller on existing architecture, rather than introducing new infrastructure to the system. This yields benefits to speed of adoption and cost. The concepts discussed for DC systems were translated to a physical AC system. Experimentation established a baseline for droop mode, tested performance with optimal generator selection, and tested the feasibility of changing droop parameters.

The optimization presented effectively regulated the voltage within 2% deviation, providing a reliable and stable output. This deviation occurred on the transitions during generator hand-off as was expected. In Region 5, the optimal mix region, the bus voltage deviated less than 0.1% and less than 0.01% compared to the conventional droop control. Although the performance is acceptable, it could be improved through energy storage integration as discussed in [5]. In the physical system, the transients were much greater but still within standards. The implementation of optimal generator selection was shown to produce acceptable performance even without ramping the power to create a soft turn off/ on. Implementing the frequency offset control did not affect stability and effectively distributed the load according to analytical calculations. Changing the frequency droop line slope created instability and had to be further adjusted using an offset, effectively rendering the method useless for power distribution.

Although the proposed control algorithm was 12.06% more efficient, the majority of the efficiency came from loads less than 60 kW. For loads greater than 60 kW, the greatest theoretical efficiency was 1.6%. Although this still equates to savings and reduced logistics, the scale in the application limits the actual realized savings. For a two generator system, the greatest investment for optimization lies in the region below where both generators operate, $P_{load} < 60$ kW. Experimentation showed that the generators can

effectively cycle on and off without exceeding specifications. Additionally, the physical generators have a larger capacity than the rated capacity, allowing for large momentary changes in the load. The generators are capable of running at 100% capacity in stand-alone, but should maintain the 80% spinning reserve as the efficiency gains are marginal past this point and frequent over-current events degrade the generator. The proposed optimization focused on changing the slope of the droop lines, whether DC voltage droop or AC frequency droop. Experimentation showed this is a less effective and stable method. The desired power distribution is more effectively achieved through changing the offset of the droop line. The optimization presented has the potential to create greater savings based on individual generator efficiencies and accuracy in modeling its continuous efficiency curve. Use of a non-linear fuel consumption curve presents minimum points that can be leveraged to achieve greater efficiencies across the entire load spectrum. The addition of multiple generators also introduces even more minimums and increases the margin for optimization.

There are three primary areas for future work: 1) AC System Modeling, 2) Multiple generators, 3) Energy Storage, 4) Further Experimentation. These proposed research areas are described below.

The system presented was a DC microgrid, but current military power systems are all AC as seen in experimentation. The underlying droop control concept remains but utilizes different control signals to account for active and reactive power. To accurately simulate the effects of this control, an AC system should be modeled to account for the difference in outputs and generator dynamics presented in experimentation. One of the secondary goals for experimentation was to gather data from which AC modeling can more effectively be done.

This thesis focused on a small, mobile tactical power system where two medium size generators were adequate for the demand. As discussed, the optimization algorithm when both generators operate is only a marginal increase in efficiency. Every additional generator beyond however creates more windows for optimization and should be explored for larger more static military locations.

Energy storage provides several layers to improving the system. Adding batteries and super-capacitors could potentially remove the need for buffer regions and allow for generators to run to max capacity, increasing efficiency even more. The batteries also provide a way to maximize a generator output and charge batteries for later use. Energy provided from batteries can not only add efficiency but also tactical advantages when reduced noise and heat signatures are needed.

Experimentation presented in this thesis established a performance baseline for the different optimization methods but did not provide a rigorous performance evaluation. Future experimentation should identify the worst case scenarios for the given optimization methods and validate adequate performance under these conditions. In addition to a generator only system, solar panels and energy storage can be integrated. Short duration tests can be done to validate worst case scenario performance. Longer duration testing can be done to test effectiveness of optimal control algorithms with a greater time horizon.

THIS PAGE INTENTIONALLY LEFT BLANK

APPENDIX A. MATLAB CODE

A. OPTIMIZATION SCRIPT

```
% Optimal Fit for Fuel Consumption Plots
clc
close all
clear
run('fit_30_60')
%% Cost Equation

P30 = linspace(0,30,300);
P60 = linspace(0,60,300);
% 30kW
Load_30 = 30*[0.25, 0.5, 0.75, 1];
galHr_30 =  [0.9, 1.23, 1.8, 2.46];
f30 = 0.6364*exp(P30*5*10^(-5));
m30 = ((1.23-0.9)/7.5 + (1.8-1.23)/7.5 + (2.46-1.8)/7.5)/3.;
b30 = 0.3;
f30 = m30*P30 + b30;

% 60kW
Load_60 = 60*[0.25, 0.5, 0.75, 1];
galHr_60 = [1.59 2.47 3.51 4.47];
m60 = ((2.47-1.59)/15 + (3.51-2.47)/15 + (4.47-3.51)/15)/3;
b60 = 0.6;
f60 = m60*P60 + b60;

figure(1)
clf
plot(Load_30,galHr_30,'*', Load_60, galHr_60,'*')
hold on
plot(P30,f30,P60,f60)
title('Consumption (gal/hr)')
grid

zStar = 30;         % Less Efficient to Run the 30kW past this point

% Iterate values of gamma for every value of P
costAtAllP = [];
costAtP_i_out = [];
C_min = [];
C_out = [];
P_out = [];
P_out130 = [];
P_out160 = [];
P_out1Total = [];
P_out230 = [];
P_out260 = [];
P_out2Total = [];
gamma = [];
g_min = [];
```

```
% Load Min and Max Gamma Values
load('gammaMin_Max');

for ii = 1:1:30
    costAtP_i_out = [];
    gout = [];
    P = 60 + ii;
    P_out = [P_out,P];
    gamma_min = gamma(ii,1);
    gamma_max = gamma(ii,2);

    length = 10;
    temp = linspace(gamma_min,gamma_max,length);
    int = temp(2)-temp(1);
    if int > 0
        for jj = gamma_min:int:gamma_max
        g = jj;
        P30 = g*P;
        P60 = (1-g)*P;

        f30 = m30*P30 + b30;
        f60 = m60*P60 + b60;
        costAtP_i = f30 + f60;                                  % Total
cost for each gamma at a given P
        costAtP_i_out = [costAtP_i_out, costAtP_i];               %
Stored Vector for the cost function
        P_out130 = [P_out130, P30];
        P_out160 = [P_out160, P60];
        P_out1Total = [P_out1Total, P60+P30];
        gout = [gout, g];
        end

    else
        for jj = 1:1:10
        g = gamma_max*(jj/jj);
        P30 = g*P;
        P60 = (1-g)*P;

        f30 = m30*P30 + b30;
        f60 = m60*P60 + b60;
        costAtP_i = f30 + f60;                                  % Total
cost for each gamma at a given P
        costAtP_i_out = [costAtP_i_out, costAtP_i];               %
Stored Vector for the cost function
        P_out130 = [P_out130, P30];
        P_out160 = [P_out160, P60];
        P_out1Total = [P_out1Total, P60+P30];
        gout = [gout, g];
        end
    end
    [minCost,minIndex] = min( costAtP_i_out);
    C_min = [C_min, minCost];
    g_min = [g_min,gout(minIndex)];
```

```
    figure(3)
    title('Cost for all Gammas at P(i)')
    plot(costAtP_i_out)
    hold on

    figure(4)
    plot(P_out130)
    title('30kW Power')
    hold on

    figure(5)
    plot(P_out160)
    title('60kW Power')
    hold on

%C_out = [C_out;costAtP_i_out];
 end

figure(6)
clf
plot(P_out, C_min)
title('Minimum Cost (gal/kWh)')
xlabel('Power')
ylabel('Cost (gal/kWh)')
grid


figure(7)
clf
plot(P_out, g_min)
title('Optimal Gamma')
xlabel('Load Power (kW)')
ylabel('\gamma_o_p_t')
save('optGamma.mat','g_min')
grid

figure(8)
clf
P30 = g_min.*P_out;
P60 = (1-g_min).*P_out;
plot(P_out,P30, P_out,P60)
grid

P30_initial = 0:1:23;
P30_B1 = (1/3)*(24:30);
P30_middle = zeros(1,17);
P30_B2 = (1/3)*(48:60);
P30 = [P30_initial,P30_B1,P30_middle,P30_B2,P30];

P60_initial = zeros(1,23);
P60_B1 = (2/3)*(24:30);
P60_middle = (31:48);
P60_B2 = (2/3)*(48:60);
P60 = [P60_initial,P60_B1,P60_middle,P60_B2,P60];
```

```
figure(9)
load('Report_gamma_total')
Pload = 1:1:90;
P30 = Pload.*gamma_total;
P60 = Pload.*(1-gamma_total);

plot(P30)
hold on
plot(P60)
hold on
plot((P30 + P60),'--k')
legend('30kW','60kW','Total','Location','best')
title('Optimal Generator Output')
xlabel('Load Power (kW)')
ylabel('Generator Power Output')
grid

figure(10)
plot(Pload,gamma_total)
title('Optimal Gamma (Full Load Profile)')
xlabel('Load Power (kW)')
ylabel('\gamma(P_l_o_a_d)')
grid

% Compare Fuel Costs
fuel30_const = m30*(Pload*1/3) + b30;
fuel60_const = m60*(Pload*2/3) + b60;
fuel_const = fuel30_const + fuel60_const;

load('fuelConstant')
fuel30_opt = (m30*P30 + b30).*(tempFuel1);
fuel60_opt = (m60*P60 + b60).*(tempFuel2);
fuel_opt = fuel30_opt + fuel60_opt;

figure(11)
plot(Pload,fuel_const, Pload,fuel_opt)
title('Fuel Consumption Comparison')
xlabel('Load Power (kW)')
ylabel('Fuel Consumption (gal/hr)')
legend('Constant Gain', 'Optimal Gain')
grid on

% Percent savings
percDiff_fuel = ((fuel_const - fuel_opt)./fuel_const)*100;

figure(12)
plot(Pload,percDiff_fuel)
title('Fuel Savings Comparison')
xlabel('Load Power (kW)')
ylabel('Fuel Saved (%)')
grid on
```

B. MODEL INITIALIZATION SCRIPT

```
%% Dommert, Initial Script
%% SETUP
clc
clear all
close all
%% PARAMETERS
tstep = 1e-3;
dec_data = 10;          % data decimation for outputs
tstep_control = 1;    % this will ensure the simulation takes off
before add optimization
fc_lpf = 1/(3);
tau_load = 1/(2*pi*fc_lpf);    % time constant for load filter

% these are used for the droop control
% 380V SYSTEM
v_perc = 0.05;                          % perc +/- for Vbus, (works
with 1%)
v_bus_ref = 380;
v_bus_max = v_bus_ref*(1 + v_perc);             % 400
v_bus_min = v_bus_ref*(1-v_perc);             % 360

delta_V = v_bus_max-v_bus_min;
%% Generators
gen_limit = 0.9;           % max amount of power use from gensets
% Generator Time Constant
current_filter = 1;       % 1 = current LPF ON, 0 = No Current LPF
tau_gen = 2;

% 30kW gen
P_30kW_max = 30000;                                 % W
i_30kW_max = P_30kW_max/v_bus_ref;
ri_30kW = 1;                                       % ohms (internal
resistance)
rv_30kW = delta_V/i_30kW_max;                       % ohms (virtual
resistance for droop control)
rv_30kW_max = delta_V/(i_30kW_max*(1-gen_limit)); % this will set the
gen "idle state"
% 30kW Fuel
Load_30 = 30*[0.25, 0.5, 0.75, 1];
galHr_30 =  [0.9, 1.23, 1.8, 2.46];
m30 = ((1.23-0.9)/7.5 + (1.8-1.23)/7.5 + (2.46-1.8)/7.5)/3.;
b30 = 0.3;
%f30 = m30*P30 + b30;  gal/kWh

save('rv_30kW','rv_30kW')
% 60kW gen
P_60kW_max = 60000;                                 % W
i_60kW_max = P_60kW_max/v_bus_ref;
ri_60kW = 2;                                       % ohms (internal
resistance)
rv_60kW = delta_V/i_60kW_max;                       % ohms (virtual
resistance for droop control)
```

```
rv_60kW_max = delta_V/(i_60kW_max*(1-gen_limit)); % this will set the
gen "idle
% 60kW fuel
Load_60 = 60*[0.25, 0.5, 0.75, 1];
galHr_60 = [1.59 2.47 3.51 4.47];
m60 = ((2.47-1.59)/15 + (3.51-2.47)/15 + (4.47-3.51)/15)/3;
b60 = 0.6;
%f60 = m60*P60 + b60;  gal/Hr

% Energy Conversion
J_kWh = 2.77778e-7;             % 1J/kWh  J to kWh
save('rv_60kW','rv_60kW')

%% DROOP CONTROLLERS
% PI Gains for Current loop
alphac=1;       % closed loop desired dynamic (1st order)
Ac=0.1;         % High Freq. Attenuation. nominal = 0.1

    % 30kW Gen
kp_i30 = ri_30kW*Ac/(1-Ac);
ki_i30 = alphac*(ri_30kW+kp_i30);
    % 60W Gen
kp_i60 = ri_60kW*Ac/(1-Ac); % arbitraty
ki_i60 = alphac*(ri_60kW+kp_i60);


% PI Gains for Voltage loop (5x for all made the repsonse much cleaner
alphav=0.1; % closed loop desired dynamic (1st order)
Av = 0.1;

    % 30kW Gen
kp_v30 = Av/((1-Av)*rv_30kW)*5;
ki_v30 = alphav*(1+rv_30kW*kp_v30)/rv_30kW*5;

% 60kW Gen
kp_v60 = Av/((1-Av)*rv_60kW)*5;
ki_v60 = alphav*(1+rv_60kW*kp_v60)/rv_60kW*5;

% SECONDARY CONTROLLER (Bus Voltage Control)
kp_v_secondary = 50;                % 1 = orginial
ki_v_secondary = 0.001*10;             % 0.1 = original
kd_v_secondary = 0;                 % 0 = original
N_secondary = 100;                  % filter coefficient, used for
derivative actions

%% Initial State Info (this is used for max current
state_30kW = 1;
state_60kW = 1;

%% LOAD Values
load('Load')
P_load = 6*P_load;
```

```
tstop = t_load(length(t_load));

maxPload =  max(P_load)
R_load_inv = (1./(P_load/v_bus_ref^2));
i_total_max =  i_60kW_max*state_60kW + i_30kW_max*state_30kW;

R_min = v_bus_max/i_total_max;
load_min = 1/R_min;


% LOAD Virtual Resistance for Optimal Update LUT
load('rvData_Mar6')

%% RUN THE MODEL with BOTH CASES
totalFuel = [];         % Initialize values for comparison
error_max = [];

%% TERTIARY CONTROLLER
opt_control = 1;            % 1 = Constant Droop, 0 = opt droop
sim('TwoGens_model_Mar7')
%% PLOT
run('TwoGens_plot_Mar7')

opt_control = 0;            % 1 = Constant Droop, 0 = opt droop
sim('TwoGens_model_Mar7')
%
% %% PLOT
run('TwoGens_plot_Mar7')
run('fuelCompare')
```

THIS PAGE INTENTIONALLY LEFT BLANK

APPENDIX B. SIMULINK MODEL

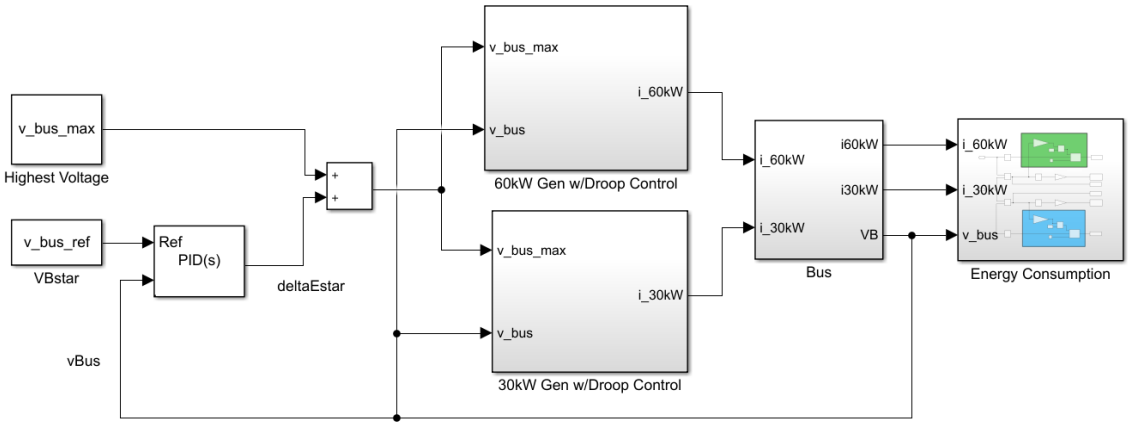

Figure 51. Parallel Generator Model

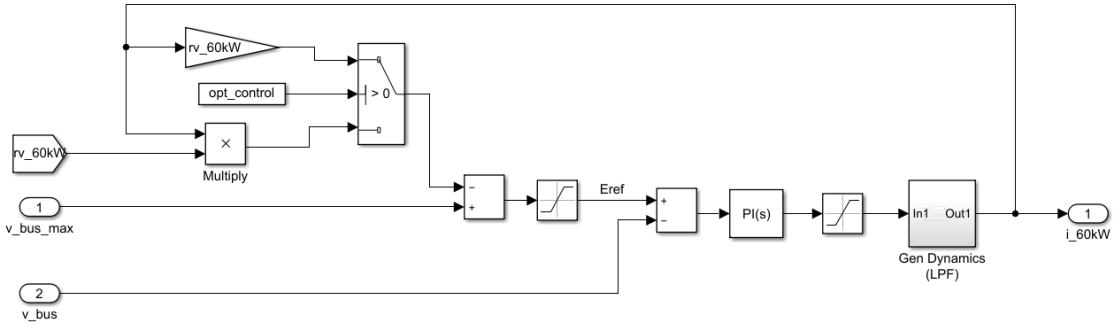

Figure 52. Generator Model with Droop Control

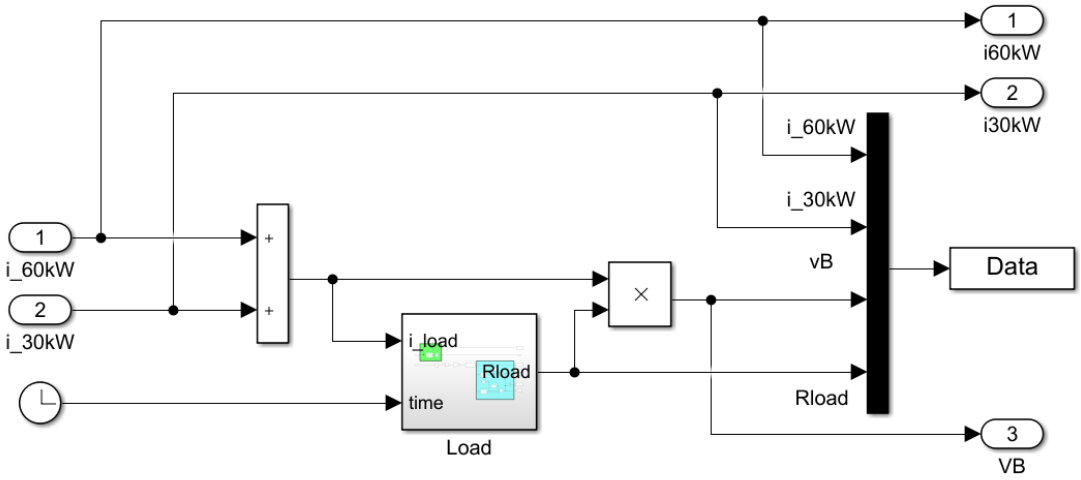

Figure 53. Bus Model

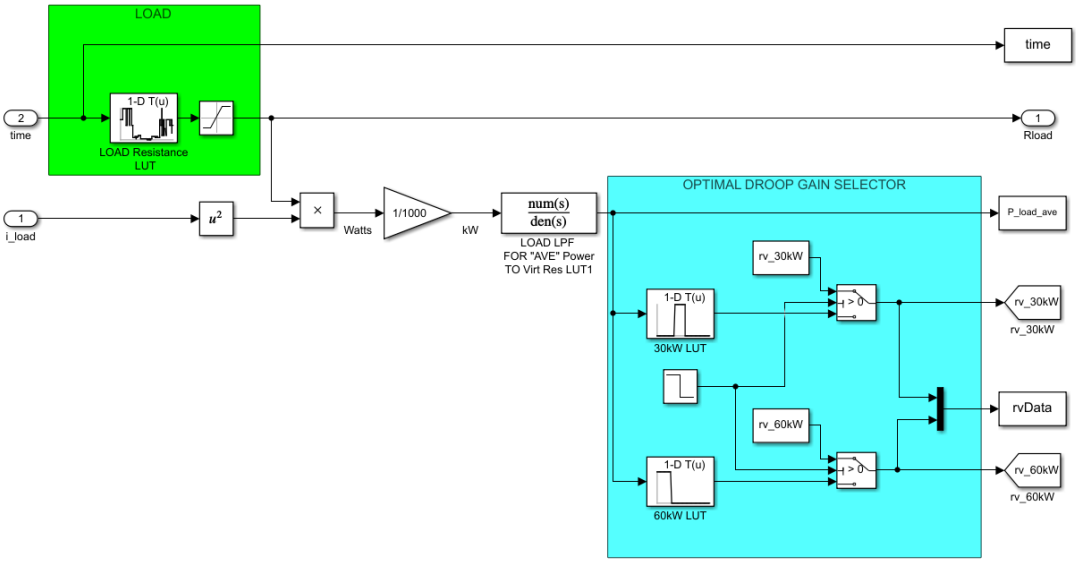

Figure 54. Load Model with Optimal Droop Gain Selector

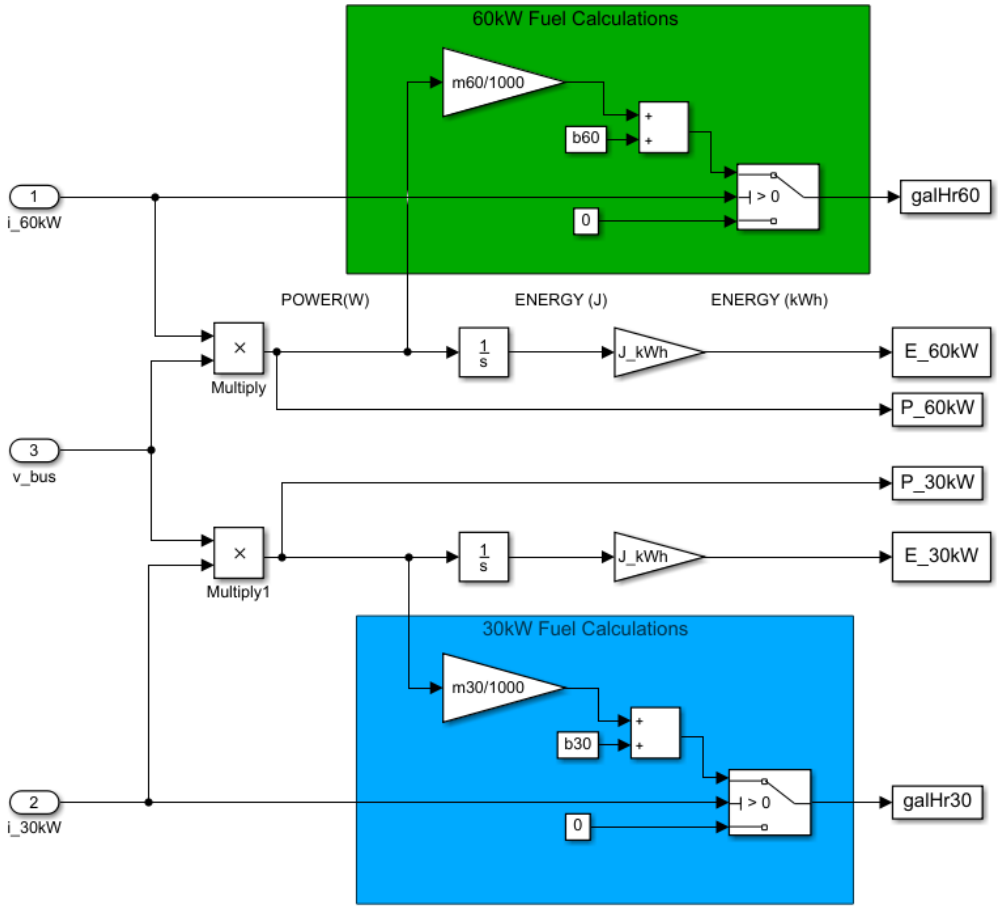

Figure 55. Energy and Fuel Calculation

THIS PAGE INTENTIONALLY LEFT BLANK

LIST OF REFERENCES

[1] *Summary of the 2018 National Defense Strategy of the Unites States of America*, United States Department of Defense, 2018. [Online]. Available: https://dod.defense.gov/Portals/1/Documents/pubs/2018-National-Defense-Strategy-Summary.pdf

[2] R. Tiron, "$400 per gallon gas to drive debate over cost of war in Afghanistan," The Hill. [Online]. Available: http://thehill.com/homenews/administration/63407–400gallon-gas-another-cost-of-war-in-afghanistan.

[3] Marines.mil, "Expeditionary advanced base operations," Accessed: May 3, 2019. [Online]. Available: https://www.candp.marines.mil/Concepts/Subordinate-Operating-Concepts/Expeditionary-Advanced-Base-Operations/,/

[4] Title 10. Armed Forces, U.S.C. section 2926, 1956.

[5] R. L. Kelly, "Optimizing gas generator efficiency in a forward operating base using an energy management system," M.S. thesis, ECE dept., NPS, 2013. [Online]. http://hdl.handle.net/10945/34686

[6] K. E. Garcia, "Optimization of microgrids at military remote base camps." M.S. thesis, Applied Mathematics, NPS, 2017. [Online]. http://hdl.handle.net/10945/56923

[7] N. Anglani, G. Oriti, and M. Colombini, "Optimized energy management system to reduce fuel consumption in remote military microgrids," *IEEE Trans on Industry Applications*, vol. 53, no. 6, Nov/Dec 2017.

[8] R. L. Kelly, G. Oriti and A. L. Julian, "Reducing fuel consumption at a remote military base: Introducing an energy management system.," in *IEEE Electrification Magazine*, vol. 1, no. 2, pp. 30–37, Dec. 2013. doi: 10.1109/MELE.2013.2293182

[9] E. Kiser, "The impact of technologies and missions on contingency base fuel consumption," M.S. thesis, Applied Mathematics, NPS, 2018. [Online]. https://calhoun.nps.edu/handle/10945/59699

[10] I. U. Nutkani, W. Peng, P. C. Loh and F. Blaabjerg, "Cost-based droop scheme for DC microgrid," *2014 IEEE Energy Conversion Congress and Exposition* (ECCE), Pittsburgh, PA, 2014, pp. 765–769. doi: 10.1109/ECCE.2014.6953473

[11] I. U. Nutkani, P. C. Loh and F. Blaabjerg, "Cost-based droop scheme with lower generation costs for microgrids," *2013 IEEE ECCE Asia Downunder*, Melbourne, VIC, 2013, pp. 339–343. doi: 10.1109/ECCE-Asia.2013.6579118

[12] I. U. Nutkani, P. C. Loh, P. Wang and F. Blaabjerg, “Autonomous droop scheme with reduced generation cost,” in *IEEE Transactions on Industrial Electronics*, vol. 61, no. 12, pp. 6803–6811, Dec. 2014. doi: 10.1109/TIE.2014.2314056

[13] “Hybridization tradeoffs,” Naval Sea Systems Command (NAVSEA) Warfare Centers Carderock, U.S. Navy, Bethesda, MD.

[14] P. C. Krause, O. Wasynczuk, and S.D. Sudhoff, *Analysis of Electrical Machinery and Drive Systems*, 2nd edition. Piscataway, NJ: IEEE Press, 2002.

[15] A. Kwasinski and R. S. Balog *Microgrids and Other Local Area Power and Energy Systems*. Cambridge University Press, 2016.

[16] Definitions of tactical, prime, precise, and utility terminologies for classification of the DoD mobile electric power engine generator set family, MIL-STD-1332B, 24 May 1971. [Online] Available: https://quicksearch.dla.mil/qsSearch.aspx

INITIAL DISTRIBUTION LIST

1. Defense Technical Information Center
   Ft. Belvoir, Virginia

2. Dudley Knox Library
   Naval Postgraduate School
   Monterey, California